SOME CHARACTERISTICS OF AN ELECTRICAL DISCHARGE TRANSVERSE TO A SUPERSONIC SEEDED NITROGEN PLASMA STREAM WITH COLD-COPPER ELECTRODES

K. E. Tempelmeyer, J. M. Whoric,
L. E. Rittenhouse and M. L. McKee
ARO, Inc.

March 1965

PROPULSION WIND TUNNEL FACILITY
ARNOLD ENGINEERING DEVELOPMENT CENTER
AIR FORCE SYSTEMS COMMAND
ARNOLD AIR FORCE STATION, TENNESSEE

NOTICES

When U. S. Government drawings specifications, or other data are used for any purpose other than a definitely related Government procurement operation, the Government thereby incurs no responsibility nor any obligation whatsoever, and the fact that the Government may have formulated, furnished, or in any way supplied the said drawings, specifications, or other data, is not to be regarded by implication or otherwise, or in any manner licensing the holder or any other person or corporation, or conveying any rights or permission to manufacture, use, or sell any patented invention that may in any way be related thereto.

Qualified users may obtain copies of this report from the Defense Documentation Center.

References to named commercial products in this report are not to be considered in any sense as an endorsement of the product by the United States Air Force or the Government.

SOME CHARACTERISTICS OF AN ELECTRICAL DISCHARGE TRANSVERSE TO A SUPERSONIC SEEDED NITROGEN PLASMA STREAM WITH COLD-COPPER ELECTRODES

K. E. Tempelmeyer, J. M. Whoric,
L. E. Rittenhouse and M. L. McKee
ARO, Inc.

AF - AEDC
Arnold AFS Tenn

FOREWORD

The work reported herein was done under Program Element 62410034, Project 7778, Task 777805. The results of the research were obtained by ARO, Inc. (a subsidiary of Sverdrup and Parcel, Inc.), contract operator of the Arnold Engineering Development Center (AEDC), Air Force Systems Command (AFSC), Arnold Air Force Station, Tennessee, under Contract AF40(600)-1000. The work was done under ARO Project No. PL2287, and the report was submitted by the authors in August 1964.

The authors gratefully acknowledge the assistance of a great number of people who participated in various phases of this work. In particular, they would like to thank A. K. Windmueller, who guided the program in its early stages; Walter Harmon, who designed a large portion of the test equipment; Don Wilson and Joe Pigott, who assisted in many ways in the assembly of the test apparatus and during the course of the tests; and Dr. J. B. Dicks for many helpful comments and suggestions during the entire course of the study.

This technical report has been reviewed and is approved.

Donald A. Vogt
Captain, USAF
Chief, Experimental Branch
DCS/Plans and Technology

Donald D. Carlson
Colonel, USAF
DCS/Plans and Technology

ABSTRACT

Some characteristics of a steady, direct-current electrical discharge transverse to a supersonic seeded nitrogen plasma are presented. The discharge from cold-copper electrodes had an overall voltage-current characteristic which was positive in all cases. The effects of (1) the type of seed (K_2CO_3 or NaK), (2) the seeding rate (about 0.2 to 2 percent K or NaK by weight), (3) the static pressure level (from 0.3 to 1.0 atm), and (4) the plasma enthalpy level (from about 1250 to 1800 kcal/kg) on the discharge are given in figure form. Dynamic data were also recorded and demonstrate that rather large fluctuations having frequencies of a few hundred cps exist in the current.

It is proposed that the electrodes introduce electrons into the conducting plasma through field emission. The discharge appears diffuse in the core of the plasma and may be quantitatively explained with an existing nonequilibrium, elevated-electron temperature theory.

CONTENTS

ILLUSTRATIONS

NOMENCLATURE

A	Electrode surface area
B	Magnetic flux density
D	Nozzle exit diameter
E	Electric field strength
E'	Electric field strength in plasma core
e	Electronic charge
h	Enthalpy
$h_{o_{local}}$	Local stagnation enthalpy measured with enthalpy probe
I	Current
J	Current density
k	Boltzmann's constant
L	Geometric spacing between opposing electrodes
M	Mach number
N	Number of samples
n	Number density
p	Pressure
Q	Collision cross section
S	Seeding rate, ratio of potassium or NaK weight flow to the total weight flow
T	Temperature
U	Velocity
V	Voltage
V_B	Induced voltage (UBL)
X	Axial distance downstream of nozzle
W_g	Arc-heater mass flow rate
Z	Horizontal distance across plasma
δ	Energy loss coefficient

σ	Electrical conductivity
ϵ_o	Permittivity of free space

SUBSCRIPTS

1, 2, 3, 4,	Electrode number
app	Applied
ave	Average
$\mathbb{Q}$	Centerline
ch	Channel
dc	Direct current
e	Electron
ei	Electron ion
ex	Exit
i	Running index
rms	Root mean square
s	Point at which $I \longrightarrow 0$
o	Stagnation or stilling chamber

SECTION I
INTRODUCTION

Electrical discharge phenomena in quiescent gases has been the subject of extensive analytical and experimental investigation for over the past sixty years and is reasonably well understood. References 1 and 2 are examples of available reference works on this subject.

In contrast to the bulk of data which exists for d-c electrical discharges in cold quiescent gases, little is known about d-c electrical discharges in a high-temperature moving plasma and particularly for plasmas having supersonic velocities. Such discharges do not necessarily behave in the classical manner of quiescent gas discharges because the gas itself is an electrical conductor and because of the mutual interaction between the discharge and the moving stream.

There are two general types of d-c discharges in moving gases which are currently being investigated. The first of these, arc discharges generally at subsonic speeds, is receiving the most attention because of the application of arcs in heating gases to high temperatures. Reference 3 contains a recent survey of some of this work. In addition, discharges transverse to both subsonic and supersonic plasma flows are being studied because of their application in magnetohydrodynamic (MHD) devices; this report is concerned with this latter type.

Some information concerning such discharges has been obtained from experiments designed to measure electrical conductivity of plasmas and from MHD experiments. References 4 through 17 describe a portion of these recent experiments; yet, only a little is known about such discharges. At the present, one must rely on experiments to empirically scratch at the surface of this field.

Results obtained from the study of electrical discharges with cold-copper electrodes transverse to a nitrogen plasma at supersonic speeds are described herein. These tests were conducted as part of a program undertaken at the Propulsion Wind Tunnel (PWT), AEDC, AFSC to develop a steady-flow $\vec{J}x\vec{B}$ accelerator for a gas-dynamic testing facility. Being a by-product of a development program, the present tests did not comprehensively study the effects of all parameters which influence the discharge; nevertheless, the influence of some factors has been determined and some interesting trends have been observed. Electrical discharges carrying currents up to 100 amp/cm^2 were achieved across a nitrogen plasma seeded with potassium. The plasma has a static temperature between about 2500 and 3500°K, a pressure between about

0.3 and 1 atm, and a velocity of about 2000 m/sec (M = 1.8). Five or six pairs of smooth segmented, water-cooled copper electrodes were employed for the tests, and, in some instances, a magnetic field was applied mutually orthogonal to the direction of the plasma velocity and applied electric field. Both steady-state and dynamic test results are presented.

SECTION II
APPARATUS

A schematic of the test apparatus is shown in Fig. 1, and Fig. 2 contains some photographs of part of the actual installation. Details of the individual components are contained in the following sections.

2.1 ARC HEATER

A vortex stabilized d-c heater was used to generate the nitrogen plasma test medium. The plasma from the arc heater passed through a small stilling chamber, seed injection flange, and supersonic nozzle before flowing into the test channel.

Several arc-heater configurations were employed during the course of these tests; typical thermodynamic states produced in the plasma are summarized in Fig. 3. Plasma enthalpies in the stilling chamber and at the nozzle exit have been obtained from a conventional energy balance.

2.2 SEEDING SYSTEMS

2.2.1 Powder Seeder

Initially, potassium carbonate (K_2CO_3) was used as the seed material and was introduced in powdered form from the seed injection flange (see Fig. 1) through a wall orifice. The powdered seed was placed in a hopper which was equipped with a constant-speed, variable-pitch augering mechanism so that the powder could be metered into a nitrogen carrier gas (Fig. 4). Average seeding rates were measured by weighing the powder in the seed hopper before and after a series of runs. Seeding rates stated herein correspond to the percentage of potassium injected into the N_2 plasma by weight.

A variation of this system was also used in which the auger was removed and the nitrogen carrier gas was forced up through the powder

bed. The powder was agitated by motor-driven stirrers so that it could be entrained by the carrier gas and carried out of the top of the hopper to the seed injection flange.

Neither system could be made to produce smooth seed injection rates.

2.2.2 Water Solution Seeder

Because seeding rates with the powder system were very erratic, a second system was assembled which sprayed an aqueous solution of K_2CO_3 into the arc-heater stilling chamber. A small reservoir was filled with seed solution, usually 50-percent K_2CO_3 and 50-percent H_2O by weight. High-pressure nitrogen was used to pressurize this reservoir and force the solution through a small wall orifice in the seed injection flange. Seed rates were again measured by weighing the amount of solution in the tank before and after a series of runs, but quoted seed rates correspond to the percentage of potassium injected into the N_2 plasma by weight. Figure 5 shows a schematic of this system and the injection conditions employed for these tests.

2.2.3 NaK Seeder

A third seeding system was also used in which a sodium-potassium alloy (NaK) was injected into the arc-heater stilling chamber through the seeding flange. This material is a liquid metal at standard atmospheric conditions; it burns spontaneously upon exposure to air or oxygen and reacts violently if brought in contact with water. Despite its unfavorable handling characteristics, it is a desirable seeding material because both the Na and K have low ionization potentials and the compound is inexpensive and liquid. The alloy used consisted of 78-percent K and 22-percent Na by weight.

The operational principle of the NaK seeder is essentially the same as described above for the water-solution seeder. However, the system itself, shown in the background of Fig. 2b, is considerably more complicated because of the necessity of purging all of the NaK lines, valves, etc. Flow rates for the NaK were measured at each data point by a turbine-type flowmeter. Seeding rates stated herein for NaK seeding correspond to the percentage of NaK flow by weight to the total plasma weight flow.

2.3 ARC-HEATER EXIT NOZZLE

From the stilling chamber, the seeded plasma passed into a convergent-divergent nozzle (see Fig. 6). This nozzle was water-cooled,

had an area ratio of 1.345, and a square exit geometry (2.54 by 2.54 cm). For some tests, a water-cooled nozzle-extension section (shown in Fig. 7) was used which had parallel sidewalls with the top and bottom walls diverged 1°15'.

2.4 TEST CHANNELS

Six channels containing either five or six pairs of electrodes were built and tested during the course of this study; however, only the test results from the last four will be presented. For convenience, these last four channels will be referred to hereafter by number as noted below. Channel 1 was connected directly to the nozzle, while the nozzle extension was used with Channels 2, 3, and 4.

2.4.1 Channel 1

Five pairs of water-cooled copper electrodes of the geometry shown in Fig. 6 were employed in this channel. Four sides of these electrodes as well as part of the top were plasma sprayed with beryllium oxide (BeO) to a thickness of about 0.5 mm, thus making the insulation an integral part of the electrode. Water flow rates of about 0.4 gpm were supplied to each electrode. The exposed copper surface of the electrode was 2.54 by 0.20 cm. A relatively smooth surface resulted when the electrodes were sandwiched together to form a constant-area channel. Insulated water-cooled copper plates were used for sidewalls. One sidewall was also sprayed with BeO, while the other sidewall was covered with boron nitride. The electrodes and sidewalls were mounted on a micarta frame.

2.4.2 Channel 2

Channel 2, as shown in Fig. 7, was made up of six pairs of water-cooled copper electrodes segmented by boron nitride insulators. This installation incorporated two pairs of electrically floating copper spacer blocks located between the nozzle extension and the No. 1 electrode (see Fig. 7). These blocks prevented the occurrence of discharges from the electrodes through the plasma to the nozzle, which was grounded. The electrode walls were diverged 1°15'. Parallel sidewalls were made up of water-cooled copper plates covered with strips of hot-pressed boron nitride. The electrodes were held together by a through-bolt which caused some arcing problems until it was completely encapsulated in an insulation material (nylon). Each electrode surface was 2.54 cm wide by 0.51 cm long.

2.4.3 Channel 3

Removal of the sidewalls of Channel 2 resulted in Channel 3.

2.4.4 Channel 4

Only five pairs of electrodes having the same geometry as those of Channel 2 were used in this configuration; however, an additional short spacer block was inserted between the two existing spacer blocks as shown in Fig. 8. Hot-pressed boron nitride slabs were used for insulation between the electrodes. Because of erosion, they were replaced after every few runs in order to keep the electrode surface relatively smooth. A divergence of 1° 15' was also used for these electrode walls.

Channel 4 was installed inside of the exhaust tank shown in Fig. 1. Initially, it was equipped with temporary sidewalls and the average static pressure in the channel was measured for various running conditions. Then, for the discharge tests, the sidewalls were removed and the pressure in the exhaust tank was adjusted to the appropriate value such that the semifree jet would be confined to the channel.

2.5 ELECTRODE POWER SUPPLY

Electrical power for the electrodes was provided by an array of 400 twelve-volt automotive-type batteries which have a 20-hr amp-hr rating of 80. Each electrode circuit was electrically isolated from the others. The system is capable of providing 384 v to each electrode pair with a minimum voltage adjustment increment of 2 v. A schematic of the electrical system and appropriate metering circuits is shown in Fig. 9a. In addition, the voltage drop in the circuit as a function of current is shown in Fig. 9b to provide an insight into the operating voltage when only the applied voltage is presented in the figures. No external ballast is provided in the battery circuit, and the voltage drops shown in Fig. 9b are due to the line resistance and internal resistance of the battery.

2.6 MAGNET

A conventional C-shaped electromagnet with rectangular pole pieces measuring 7.6 by 38.1 cm and with a pole gap of 6 cm was used during some of these experiments (see Fig. 10a). The maximum field obtainable with this magnet is about 20,000 gauss, and the field distribution on the centerplane is shown in Fig. 10b. The location of the channel relative to the magnet is also shown in the figure.

2.7 INSTRUMENTATION

Steady-state electrode voltages and currents were indicated on panel meters. Voltage dividers together with 10-mv meters were used to provide a full-scale deflection of 200 or 500 v. Current meters were used in conjunction with 50-mv shunts and had a full-scale reading of 100 amp. These meters were also used with appropriate shunts to measure currents in the range from 0.01 to 1 amp. All meters were calibrated, and the presented data have been corrected accordingly. Steady-state electrical data were continuously recorded by photographing the meters with a 70-mm sequence camera at the rate of one frame per second.

Nonsteady current and voltage data were recorded on a magnetic tape system at a tape speed of 60 in./sec with a 10-kc response. These data were then reproduced on an oscillograph trace at 1/8 and 1/32 of the recorded speed. Dynamic data were directly recorded on an oscillograph for some of the tests.

Wall static pressures were measured (1) in the stilling chamber, (2) at the exit of the nozzle extension section, and (3) just upstream of the first electrode pair. Also, stagnation pressure measurements were made at the nozzle exit with an impact pressure probe, and the pressure profiles were recorded on a millivolt recorder.

Stagnation enthalpies of the plasma stream leaving the nozzle were also obtained with an enthalpy probe. Details of this probe and its method of operation are contained in Ref. 18. It was also utilized for some impact pressure measurements.

Cooling-water flow rates to the anodes, cathodes, and sidewalls were individually measured with turbine-type flowmeters. Also, water temperature rises were obtained with conventional thermocouples so that heat-transfer rates to the electrodes could be determined from thermal balances.

Additional instrumentation of a conventional type was provided with the arc heater which allowed a determination of the bulk enthalpy of the plasma by means of an energy balance.

SECTION III
ACCURACY

Estimates of the overall accuracy of some of the measured test results are shown below. These estimates include such factors as the

precision of the measuring instruments, calibration errors, repeatability of test and flow conditions.

Electrode Voltage	±5 v
Electrode Current	±2 amp
Arc-Heater Enthalpy	±100 kcal/kg
Seed Injection Rate	
NaK Seed	±0.01 percent
($K_2CO_3 + H_2O$) Seed	±0.1 percent
K_2CO_3 Powder	Unknown
Channel Static Pressure	±0.05 atm
Heat-Transfer Rate	±10 percent

SECTION IV
PLASMA FLOW CONDITIONS

4.1 IMPACT PRESSURE DISTRIBUTION

Typical impact pressure distributions which were measured with a traversing probe at the exit of the nozzle extension are presented in Fig. 11. All of the impact pressures indicated that the stagnation pressure at the entrance of the test channels was reasonably uniform in the core of the plasma, but a ridge of somewhat higher pressure existed around the edge. The cause of this distribution is not known with certainty. It may be an indication of a residue vortex from the arc heater caused by the tangential gas injection method; or, it may be an effect of the severe gas cooling adjacent to the highly cooled walls. Seeding was found to have little effect on the level of the impact pressure or pressure distribution (compare Figs. 11a and b).

4.2 FLOW VELOCITY

From measurements of (1) the impact pressure, (2) the arc-heater stilling chamber pressure, and (3) the static pressure near the exit of the nozzle section, various estimates can be made for the Mach number at the entrance of the test channels. Calculations yield a range of possible Mach numbers between 1.65 and 1.85, depending upon which pressure ratio is employed and whether the flow is treated as frozen or in equilibrium. Equilibrium normal shock calculations for real-gas nitrogen probably give the most realistic results and indicate $M \approx 1.80$.

A range of entrance velocities has also been determined using the various Mach numbers indicated by the pressure measurements and the calculated enthalpies at the nozzle exit which are given in Fig. 3. Results of velocity calculations for the unseeded case are given in Fig. 12 as a function of the plasma enthalpy. When seed is injected into the plasma, the Mach number is essentially unaffected but the velocity decreases because of the attendant decrease of the plasma temperature. Approximate calculations indicate that as much as 2-percent NaK seed addition will only decrease the speed of sound and hence velocity by 3 percent. Considerably larger velocity decreases would occur with the use of K_2CO_3 seed in aqueous solution.

Also shown in Fig. 12 is an independent measurement of the plasma velocity reported in Ref. 19, which was made in the free-jet, seven nozzle widths downstream of the nozzle exit plane. This flow velocity was determined by measuring the time of flight of non-uniformities in electron density between a pair of microwave beams (see Ref. 19 for details). This measurement indicated a velocity somewhat less than that calculated at the nozzle exit. However, the microwave measuring station was considerably downstream of the nozzle exit, and when the velocity decrease is considered, the microwave data appear to support the calculated values which were obtained at the nozzle exit.

4.3 ENTHALPY DISTRIBUTION

Probe measurements of the stagnation enthalpy were made in the plasma for the unseeded case (Fig. 13). Two typical profiles are shown in the figure for different axial probe locations and arc-heater conditions. These data illustrate the reasonably good agreement between the plasma enthalpy as determined from probe measurements and the arc-heater energy balance. In one case a continuous trace was obtained, while in the other case a point-by-point measurement was made. A bulk plasma enthalpy was determined by integrating the enthalpy probe values over the flow area, taking the mass flow distribution into account. This integrated bulk enthalpy, although not presented, agreed well with the value of the plasma enthalpy determined from the arc-heater energy balance.

When the enthalpy probe was placed in a seeded flow, the seed condensed inside of the probe, thus precluding the measurement. However, the decrease of the plasma temperature resulting from seeding with various amounts of NaK has been determined by use of the energy conservation equation. Results of these calculations are summarized on the following page.

Seed Rate, S, percent	Stagnation Enthalpy, h_o, kcal/kg	Stagnation Temperature, T_o, °K	Estimated Plasma Static Temperature, T, °K
0	1833	5380	3730
0.5	1808	5340	3600
1.0	1783	5310	3540
2.0	1733	5240	3460
0	1556	4910	3090
0.5	1530	4870	3050
1.0	1505	4820	3010
2.0	1461	4725	2930
0	1278	4260	2560
0.5	1254	4190	2520
1.0	1227	4130	2480
2.0	1198	4020	2420

The plasma static temperatures were obtained by making a graphical equilibrium isentropic expansion on a real-gas nitrogen Mollier diagram.

Similar calculations have not been attempted for K_2CO_3 powder or K_2CO_3 + H_2O seeds because of the uncertainty associated with the attendant chemical reactions. Rough calculations indicate, however, that the plasma temperature for K_2CO_3 + H_2O seeding would be reduced about 200 to 400°K below the values shown in the preceding table.

Because of the uncertainties attached to estimates of the plasma static temperature, the plasma total enthalpy obtained from the arc-heater energy balance (a measured quantity) is used throughout this report to characterize the test data. If desired, one can estimate the plasma temperature from the stated enthalpy level and seeding rate by using the values in the above table for NaK seed and by applying an additional 200 to 400°K reduction for K_2CO_3 + H_2O seed.

SECTION V
RESULTS AND DISCUSSION

5.1 DISCHARGE TEST RESULTS

5.1.1 Seeding Effectiveness

Seeding rates stated herein correspond to the flow rate of injected K or NaK to the total plasma flow rate. However, some seed condensed

on the cool stilling chamber, nozzle, and channel walls, so the actual seeding rates are somewhat less. There is some hope that the seed condensate layer reaches an equilibrium thickness after some time and then all of the injected seed goes into the plasma.

Electrode current data obtained by photographing the d-c ammeters at one-second intervals demonstrate the effectiveness of the seeding systems (Figs. 14, 15, and 16). As illustrated by Fig. 14a, large random current fluctuations existed in Channel 1 whenever powder seed was used. The injection rates were erratic, and the seed was poorly distributed in the plasma. The extreme fluctuations caused by powder seed were not influenced by the seeding rate, electrode material, or channel geometry.

Figure 14b contains similar discharge data also obtained with Channel 1 at nearly the same operating conditions as for Fig. 14a, but with (K_2CO_3 + H_2O) seed. In this case the discharges were found to be much steadier than those obtained with powder seed because of the considerably more uniform injection rates*. Liquid K_2CO_3 seed appears to produce a relatively slow current buildup (3 or 4 sec), and then an overshoot and return to the quasi-steady-state value. A typical current vs time plot for Channel 3 (Fig. 15) demonstrates that the magnitude of the "overshoot" decreases with an increase of the rate of seed injection. At the present, the starting transient is not understood but it seems more probably associated with the mechanics of the seed injection.

Current fluctuation data obtained with Channel 4 without sidewalls but operating at matched pressure** (0.3 atm) and with NaK seed are given in Fig. 16. With liquid NaK seed the current rises very rapidly (actually in less than 0.01 sec) in contrast to the slow starting transient which occurs when seeding with aqueous solutions of K_2CO_3; and there is, in general, no overshoot. Moreover, the electrode currents are somewhat smoother with NaK seed than with aqueous solutions of K_2CO_3.

5.1.2 Current-Voltage Characteristics without a Magnetic Field

The general characteristics of the discharge with cold-copper electrodes and the influence of several parameters on it may be illustrated

---

*A subsequent section will show that higher-frequency fluctuations, which were damped by the steady-state meters, still exist, however.

**The pressure surrounding the open-sided channel is matched to the static pressure measured in a closed channel; in which case, the jet is essentially confined to the channel even though the sidewalls are removed.

by averaged current-voltage curves (Figs. 17 through 20). Rough measurements indicated that the electrode surface temperatures were below 600°K. The current and voltage data have been averaged over time, excluding any starting transients, and then axially along the channel, but omitting data from the first and last electrodes which are subject to end effects.

In all cases the discharges established across the supersonic, seeded nitrogen plasma were characterized by a positive current-voltage characteristic, thus indicating that the discharge is not in the form of a normal arc. It is interesting to note (see Fig. 17) that although the current fluctuations were very large for powder seed, the averaged current-voltage characteristic compares well with that obtained with aqueous K_2CO_3 seed. It may be observed that the shape of the V-I curve depended primarily upon the pressure level (Fig. 20) and secondarily upon the type of seed (compare Figs. 18 and 20) and enthalpy level (Fig. 19). The seeding rate appeared to have little effect on the shape of the V-I curves (Fig. 18), but if seed injection is stopped the discharge ceases.

All of the current-voltage discharge curves appear to have a voltage intercept at zero current between about 35 and 90 v. This intercept is often interpreted in the literature as the sum of the cathode and anode sheath drops.* A more detailed examination in the current range between 0.01 and 1.0 amp (Fig. 21), however, has shown that small currents still flow at lower voltages. Thus, the curves of Figs. 17 through 20 actually become asymptotic to the voltage ordinate. The apparent voltage intercept signals the onset of a different current flow mechanism. For these tests, the point at which the current mechanism changed was found to be influenced by the plasma enthalpy level (Fig. 19), pressure level (Fig. 20), and the seeding rate (Figs. 18 and 19). These factors not only influence the apparent intercept voltage, but they also shift the entire level of the curve.

Typical current-voltage curves for individual electrode pairs in Channel 4 are presented in Fig. 22. These data have been time-averaged, and their average, omitting pairs 1 and 5, corresponds to the averaged V-I curves shown in one of the previous figures. When the discharge occurred at a pressure level of nominally 0.3 atm (Fig. 22a), the V-I curves become quite flat at currents above 40 amp and exhibit large current increases with little or no running voltage increase**. This discharge

---

*For the present case, this apparent intercept may also include voltage drops across the cooler boundary layers.

**The power supply has the drooping characteristic required for stable operation.

characteristic has also been obtained by other investigators but at much lower pressure levels (Refs. 20 and 21). It is believed that a further increase in applied voltage would probably force the discharge into the arc mode and the voltage would begin to decrease with increasing current. At higher pressures, for example, 1 atm (Fig. 22b), the V-I curves show little sign of flattening out at currents as high as 80 to 100 amp. These data tend to demonstrate that the discharge mechanism in a seeded plasma is quite sensitive to pressure level, and a discharge with a positive characteristic can be sustained at higher voltages and currents as the pressure is increased. The present data only indicate a trend in this direction and give no indication of the pressure range over which this characteristic exists.

5.1.3 Axial Distribution of Current

The axial distributions of the current carried by the various electrodes for Channels 1, 3, and 4 are presented in Figs. 23, 24, and 25. Powdered and aqueous solutions of K_2CO_3 seed produced about the same axial current distributions at a given voltage while a different axial distribution resulted when NaK seed was used (see Fig. 23). Variation of the seeding rate itself did not influence the axial distribution of currents (Fig. 24) although it did influence the level. Further, the current on the last electrode generally increases significantly because of end effects. There is a larger volume of plasma through which the discharge originating at end electrodes may pass.

During the tests with Channel 4, without sidewalls, the exhaust pressure was purposely varied to establish various shock and expansion patterns and hence axial pressure gradients in the discharge region. Although it was impossible to measure the axial pressure distributions, at least the gross effects of pressure on the discharge could be observed in this way. Some of the results of varying the pressure level are summarized in Fig. 25. When the exhaust pressure was matched to the average static pressure on the electrodes with the sidewalls installed ($p = 0.3$ atm), the jet came straight out of the channel and only weak shocks existed in the channel region. When the pressure was raised or lowered such that the semifree jet was operating in the overexpanded or underexpanded modes (in the y-direction), the axial currents were significantly altered. Both the current level and distributions varied as the pressure changed. Dimmock and Kineyko (Ref. 22) have shown that the visible "shock diamonds" are regions of high electron density in seeded rocket jets. Thus, the various axial distributions of current at different pressure levels in the present tests most probably reflect flow patterns generated in the channel. If an internal shock system and pressure gradients exist, as is currently speculated, then Fig. 25 clearly

shows the difficulty in obtaining a specified current density distribution in a MHD accelerator channel. A cross plot of the average electrode current obtained with 108 v applied to all of the electrodes is given in Fig. 26 and further illustrates this point.

5.1.4 Current-Voltage Characteristics with a Magnetic Field

Discharges were also established across the supersonic plasma in the presence of a mutually orthogonal magnetic field of about 1.55 webers/m^2 over Electrode 3 (see Fig. 10b). Orientation of the magnetic and electric fields is such that the Lorentz force acted in the downstream axial direction. Voltage-current characteristics with the magnetic field (Fig. 27) are similar to those previously shown; only, when a B-field is applied, a larger voltage is required to achieve a given current because of the necessity of overcoming the induced electromotive force (emf). This voltage increase is given by V_B = UBL, and at near-zero current it could be utilized to measure the plasma velocity. By taking the indicated plasma velocity given in Fig. 12 at h_o = 1450 kcal/kg to be uniform in the core, and by approximating the boundary layers by a linear velocity distribution from zero at the wall to the core value at the edge of the boundary layer, * one would predict an induced voltage of 85 v. This agrees well with the experimental induced voltage at near zero current; for example, at 5 amp the potential induced by the magnetic field is about 82 v. This comparison was not made at zero current as it should be because of the difficulty in accurately defining the voltage intercept.

The V-I curve with a magnetic field also exhibits a positive characteristic with little tendency to flatten out at currents up to 80 amp. The difference in the running voltage at a given current with and without a magnetic field increases with increasing current. This may, in part, be due to an increase of the plasma velocity resulting from the accelerating effect of the axial Lorentz force which increases the induced emf. But, it may also be due to a decrease of the electrical conductivity because of two tensor conductivity effects: (1) calculations contained in Ref. 23 indicate that the scalar conductivity for the conditions of these tests would be decreased about 5 percent in a channel with segmented electrodes because of ion-slip effects, and (2) if the Hall current was not exactly neutralized in this segmented channel the conductivity would be reduced even further.

---

*Both the cathode and anode boundary-layer thicknesses were estimated to be 0.5 cm from photographs.

Although discharge data were obtained for only two seeding rates, it does appear that the discharge phenomena are much more sensitive to seeding rate when a magnetic field is applied.

5.1.5 Dynamic Characteristics of the Discharge

Long-duration current fluctuation data have been presented in Figs. 14 through 16; in addition, higher frequency fluctuations also exist. Data in the previous figures were obtained from conventional d-c meters which damped any high-frequency phenomena. Higher frequency current fluctuations, however, were recorded on magnetic tape and then re-recorded on an oscillograph.

Figure 28 contains current-time traces for Electrode Pairs 2 and 3 in Channel 3 obtained with 1.5-percent potassium seed in the form of $K_2CO_3 + H_2O$. At an applied voltage of 48 v (Fig. 28a), the current was still very low (the mean was less than 1 amp) except for random occurrences of high-current bursts. This voltage level roughly corresponds to the electrode "zero" current intercept or sheath potential indicated by the previously introduced V-I curves; thus, the current-flow mechanism appears to be in a transitional state at this voltage level. It is apparent that the transition to higher current occurs sporadically. It is believed that the random current spikes are due to bursts of electrons from the cathode, probably induced by field emission as discussed in a later section. Typical current fluctuations which exist at higher voltages when $K_2CO_3 + H_2O$ seed was employed and no magnetic field applied are given in Fig. 28b. These and other dynamic data have been statistically averaged to determine the d-c current. The tape data were digitized and the currents determined from

$$I_{dc} = \frac{1}{N} \sum_{i=1}^{N} I_i$$

to provide a check with the d-c meter data. Similarly, the root-mean-square fluctuating current was calculated from

$$I_{rms} = \frac{1}{N}\left[\sum_{i=1}^{N} (I_i - I_{dc})^2 \right]^{1/2}$$

to characterize the magnitude of the fluctuations. Computed values of I_{dc} agreed well with the meter data even though the fluctuations were large, as witnessed by large computed values of the rms current. For these tests the rms current can be empirically related to the d-c current (for d-c currents above 10 amp) by

$$I_{rms} = 0.23\ I_{dc} + 5.75$$

where the units for I_{rms} and I_{dc} are amperes. Moreover, it was found that the amplitude density of the current fluctuations were distributed in roughly a gaussian manner about the d-c level. With a $K_2CO_3 + H_2O$ seed the current fluctuations had a favored frequency of 200 to 300 cps. *

Dynamic discharge data obtained with $K_2CO_3 + H_2O$ seed but also with an orthogonal magnetic field are presented in Fig. 29. These current fluctuations were not recorded on magnetic tape but on an oscillograph which had a response of 1000 cps. As a consequence, these data could not be analyzed as were the tape data. It is possible, however, to compare peak-to-peak current fluctuations. Typically, the peak-to-peak current fluctuations without a magnetic field with $K_2CO_3 + H_2O$ seed were about ±40 percent of the d-c current, while with a field of 15,500 gauss, they were reduced to about ±25 percent of I_{dc}. This decrease could be due to the diminished frequency response of the oscillograph as compared to the tape system, but it could also be caused by the diffusing effect of the B-field on the discharge. The amplitude of the fluctuations with a magnetic field is still significant.

When NaK was employed for seeding in Channel 4, the peak-to-peak amplitudes of the current fluctuations without a magnetic field were somewhat reduced to what they were with $K_2CO_3 + H_2O$ seed, but still about 30 to 35 percent of the d-c current at currents above about 50 amp (see Fig. 30). Also, the more prominent frequencies were 80 to 100 cps when NaK seed was used.

Figures 28b and 30b also show that a strong correlation exists between the current fluctuations of the various electrodes. For Channel 4 with NaK seed (Fig. 30b), it is possible to detect a time shift of the fluctuation along the electrodes by stretching out the current signal (re-recording it from the tape at much greater paper speeds). A time delay of about 4.8×10^{-5} sec** occurs between the fluctuations on Electrode Pair 1 and Electrode Pair 5. If the current flowing across the plasma passes through an area similar to that bounded by the electrode and insulator surfaces, one would define a flow velocity from the time delay by using the axial distance between these two electrodes. This assumption results in a velocity of about 600 m/sec, which is far less than the

---

*Current fluctuations in the arc heater supplying plasma to the test channels had frequencies of 5000 to 6000 cps.

**The accuracy of the system was $\pm 2 \times 10^{-5}$ sec.

free-stream velocity, and leads to the conjecture that the fluctuations arise because of some phenomena which occur in the boundary layers or because of seed material moving much slower than the stream, perhaps over the electrode surfaces.

5.2 ESTIMATION OF ELECTRICAL CONDUCTIVITY

The nonlinear shape of the current-voltage curves indicate a strong influence of the discharge on the plasma conductivity. If the electrical conductivity is identically defined by

$$\sigma = \frac{J}{E'} \tag{1}$$

and σ, as well as J are dependent on E', the electric field in the plasma core ($E - E_S$), then

$$\sigma = \frac{\partial J}{\partial E'} - E' \frac{\partial \sigma}{\partial E'} \tag{2}$$

In which case σ cannot be obtained by simply taking the slope of E vs J (or V-I) curve as is often done. Using the local slope method is equivalent to defining σ in the following manner:

$$J = \int \sigma(E')\, dE'$$

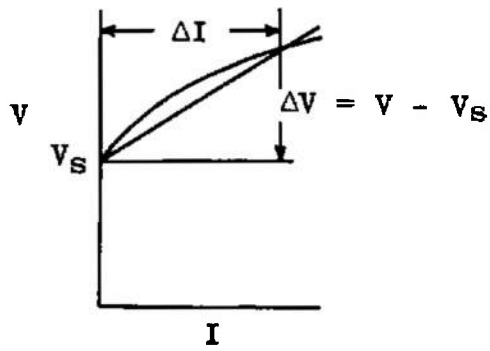

Estimated conductivities which satisfy Eq. (1) were obtained by taking the slopes of straight lines passing through V_S (that is, V at which $I \longrightarrow 0$) and points along the curve as shown in the adjacent sketch. In the present experiments the basic measurements were current and voltage, and the conductivity has accordingly been obtained from

$$\sigma = \left(\frac{I}{V - V_s}\right)\left(\frac{L}{A}\right) \tag{3}$$

where L is taken as the mean geometric spacing between opposing electrode pairs and A is taken as the electrode metallic surface area. These choices, although somewhat arbitrary, are believed to be realistic. The discharge undoubtedly expands and fills the volume of the channel between opposing insulators. In addition, photographs indicate that the discharge is blown rearward; hence, the path length over which the electrons flow is larger than the electrode spacing. These are compensating effects, but the latter is believed to be the larger. Thus, the conductivities reported herein may be somewhat conservative.

Some typical values of the conductivity obtained from faired current-voltage curves are shown in Fig. 31 and demonstrate the relatively weak dependence on seeding rate, but show a strong influence of the current density on the conductivity. However, for seeding rates lower or higher than employed during the present experiments, the dependence of conductivity on seed rate would change significantly. For these tests, 1-percent seeding appears to be about the optimum. Energy calculations forcefully show that joule heating of the entire gas by the discharge is too small to account for the increase in conductivity with increasing current. Kerrebrock (Ref. 24) has proposed the Two-Temperature Conduction Law for plasmas, which assumed that the electrons are selectively heated in the electric field and achieve temperatures greater than the gas temperature. Further, this theory assumed that the ionization is in equilibrium with this elevated electron temperature. Kerrebrock and Hoffman (Ref. 25) have experimentally demonstrated that the conductivity of potassium-seeded argon at atmospheric pressure and temperatures around 1500°K will follow the Two-Temperature Conduction Law if the electron-neutral energy exchange coefficient, δ, has the value of about ten, rather than the classical value of two for elastic collisions. This coefficient appears in the theory to describe the energy losses from the electron gas by elastic collisions with the neutrals. Zukoski, Cool, and Gibson (Ref. 26) have reported results of similar experiments with potassium-seeded argon and also find that $\delta = 2$ is somewhat small to obtain agreement between experiment and theory. They also suggest the use of higher values of δ.

There is another limitation to applying the theory as originally presented in Ref. 24 which is not inherent to the concept of the theory itself, but rather in the calculation of conductivity. Kerrebrock proposes a standard equation to compute σ which is made up of two terms; the first represents the resistivity caused by electron-neutral collisions and the second the resistivity of electron-ion collisions. The latter term arises by applying the Spitzer-Harm theory for fully ionized gases to represent the electron-ion collisions. By grouping terms in a certain way, one essentially defines an effective electron-ion cross section (see Ref. 23 for details) as

$$Q_{ei} = \frac{0.9\ e^4}{(4\pi\ \epsilon_o\ kT)^2}\ \ell n\ \Lambda$$

where

$$\Lambda = \frac{12\pi}{c^3}\left[\frac{(\epsilon_o\ kT)^3}{2\ n_e}\right]^{1/2}$$

is the ratio of the Debye length to an impact parameter for a 90-deg deflection of the electron by the ion.

Spitzer points out in Ref. 27 that his theory breaks down for values of ($\ell n\ \Lambda$) less than about five, that is, at low temperatures and/or high pressures. There has been some experimental agreement with the Spitzer-Harm theory from several sources for values of $\ell n\ \Lambda$ between 3 and 6. However, Spitzer states that this agreement is only fortuitous. Thus, in this range the concept of an effective electron-ion cross section may break down. For the theoretical calculations presented here, ($\ell n\ \Lambda$) falls in this dubious range as illustrated below:

Values of $\ell n\ \Lambda$ for Nitrogen with 1-percent (by weight) Potassium Seed

	$\ell n\ \Lambda$		
T, °K	p = 0.01 atm	p = 1.0 atm	p = 10 atm
2,000	5.56	4.58	4.09
3,000	4.51	3.46	2.97
4,000	4.51	2.98	2.43
6,000	5.37	3.27	2.36

Since the values of the effective Q_{ei} are 10^3 to 10^4 times the typical values of electron-neutral cross sections, the computed conductivity may be dominated by Q_{ei} over a wider range than actually occurs.

In a subsequent summary of the theory (Ref. 28), Kerrebrock appears to suggest considering either the electron-neutral or the electron-ion collisions to be dominant, but one still is confronted with the problem of determining when the coulomb or long-range collisions (space charge dominated) become important.

Keeping in mind the uncertainty associated with the correct value of δ and the possibility that the σ calculations may be invalid in this range, the electrical conductivity for NaK and potassium-seeded nitrogen has been calculated from Kerrebrock's steady-state two-temperature conduction model* for comparison with the experimental results. The collision cross sections (momentum exchange) used for these calculations are the same as those employed in the equilibrium conductivity calculations

*Approximate calculations by B. Curry of this laboratory (Ref. 29) indicate that the relaxation effects on non-equilibrium conductivity are not significant for the conditions of these tests.

contained in Ref. 23. Several values of the energy exchange coefficient were examined, but a δ of 100 was found to provide the best overall match to the experimental data; this is several times the δ initially suggested by Kerrebrock for nitrogen (see Ref. 24). The theoretical values for 1-percent seed (by weight) and a pressure level of 1 atm are compared in Fig. 32a to the experimental conductivities obtained at nearly the same conditions. In this case the experimental conductivities were evaluated directly from the test data rather than from faired curves. Because the plasma temperature and true seeding rate were not accurately known, a conclusive comparison is not possible. However, the level and trends of the experimental results agree at least quantitatively with the theory. A similar comparison is made for a pressure level of 0.3 atm in Fig. 32b, again with $\delta = 100$. At this lower pressure the agreement is not as good. This theory also indicates that the temperature of the electron gas is only moderately elevated above the bulk gas temperature (about 500°K at the higher current densities).

In any event, the agreement between the experimental conductivities and those predicted by Kerrebrock's theory appears reasonable, considering the uncertainties associated with both the theory and the experimental results. Thus, the Two-Temperature Conduction Law may be used to explain at least in a gross way the shape of the voltage-current curves and the conditions in the core of the plasma for the ranges covered by these experiments. Moreover, the energy exchange coefficient, δ, for seeded nitrogen appears to be about five times greater than the expected value, as has been previously found for potassium-seeded argon.

5.3 ELECTRODE PHENOMENA

Basic to the understanding of electrical discharges is a knowledge of the processes occurring at the electrodes. This section shall be devoted to that consideration, and some observed phenomena will be reported.

Photographs of the discharge (without a magnetic field) with the sidewalls removed, but the exhaust pressure matched to the average electrode pressure, always show very bright bluish-white regions attached to the trailing edges of the individual electrodes. These bright regions somewhat resemble small arcs and exist on both cathodes and anodes. They appear to be swept rearward, extend into the stream only across the boundary layers, and move in a random fashion laterally across the

trailing edges of the electrodes.* In addition to these, there are occasional bright spots which move axially across the electrodes. Movies at frame speeds up to about 3000 frames/sec indicate that the discharge is diffuse through the core of plasma free stream, however. The discharge is not self-sustained. If the seed injection is stopped, none of the electrodes carries current and all of the bright regions on the electrodes instantly disappear. Figure 33 is a photograph of the discharge which illustrates the flow pattern within the channel; however, it must be pointed out that the exit pressure was not matched to the channel pressure so that the shock patterns shown are not typical. It is not known whether oblique shock waves originate at the first electrode, whether the flow has separated, or both. In either case, it is obvious that severe pressure gradients do exist in the region of the electrodes for this operating mode.

The electrodes operate at temperatures below about 600°K and indicate little evidence of erosion after being run for long periods. Some loss of material did occur at the trailing edges, as indicated in Fig. 34a, as well as erosion of the insulation between the electrodes. It is of interest to compare the slight erosion of the water-cooled copper electrodes to the severe erosion experienced by a set of uncooled tungsten electrodes (Fig. 34b) which were used for a considerably shorter time.** Tests with the tungsten electrodes illustrate the consequences of not maintaining the temperature of thermionic emitters within the narrow range available for satisfactory operation. Some heat-transfer data obtained from a heat balance of the electrode cooling water are shown in Fig. 35. Most of the discharge tests were made over periods of 10 to 30 sec, but a few special heat-transfer tests lasting about two minutes were made where the electrode cooling water had sufficient time to reach thermal equilibrium. These results show that the electrode heating rates are moderate. When a discharge is initiated the increase of heat transfer to the anode is about twice that to the cathode, probably caused by electronic impact.

The possibility of thermionic emission has been examined as a means of supplying electrons into the plasma. Since the electrode surface temperatures are quite low, this at first glance does not appear to be a very

---

*The high-frequency current fluctuations described in Section 5.1.5 could be caused by the existence of arcs across the cooler boundary layers.

**The tungsten electrodes were designed for thermionic emission and were tested in another test channel. These results have not been included herein because of the very erratic seeding rates.

probable mechanism. Thermionically emitted current at the measured cathode temperature (taking into accout the Schottky effect) is several orders of magnitude lower than that experienced during these tests. Even if one considers the possible formation of a monolayer of an alkali metal from the seed on the electrode surface and the attendant lowering of the electrode work function, the thermionic emission current under the most favorable conditions imaginable is still far less than occurs. There is also the possibility of thermionic emission directly from the seed material or some compound formed from it. But, a study of possible chemical species which might be deposited on the electrodes indicates that these materials would vaporize and leave the electrodes at temperatures well below where thermionic emission becomes significant. Moreover, tests have been made using NaK with both clean electrodes and electrodes covered with seed which demonstrate that there is no time lag required for a seed layer to build up before current begins to flow. Thus, a brief analysis indicates that thermionic emission is not a very probable mechanism by which electrons are supplied to the stream from the cold cathodes.

Field emission is widely accepted as the primary electron emission mechanism for the low-melting-point cathodes. The field emission theory maintains that the necessary electrons are pulled free from the cathode surface by high electric field strengths formed by a sheath of positive ions very close to the cathode surface. It is generally believed that the cathode sheath thickness is roughly equal to a Debye length. For the conditions of these experiments, the Debye length is about 10^{-6} cm, which could result in electric fields of several million volts per centimeter acting on the cathode (assuming a linear variation of potential across the Debye length). With such electric fields, calculation of field-emission current densities from the Fowler-Nordhiem equation corrected for the effects of an image potential (see Ref. 30 for details) yields values which, although still lower than the measured currents, are much nearer than those predicted for thermionic emission. Murphy and Good (Ref. 31) have corrected the Fowler-Nordhiem equation to account for the contribution to the current by electrons in the cathode that are in energy states above the Fermi level because of the temperature of the cathode. Jones and Nicholas (Ref. 32) have shown that the temperature-corrected equation agrees well with experimental results if regions of low work function are assumed present on the cathode surface. The work function of the electrode material could also be depressed by the deposit of an alkali layer on the surface. The temperature-corrected emission equation of Ref. 31 does not include the image potential correction. If the combined effects of (1) the image potential, (2) the electrons with energy states above the Fermi level, and (3) the lowering of the work function by impurities on the cathode surface are considered, the measured currents

could easily be explained by field emission. In addition, there may be the possibility of some local thermionic emission because of the lowering of the work function by field emission and the much higher local surface temperatures at the areas of field emission, particularly at the points of surface irregularities. Because of the very slight erosion experienced by the cold-copper electrodes, even this amount of local thermionic emission must be small. Hence, the dominant electron emission mechanism is believed to be field emission, which is only slightly augmented by thermionic emission.

Because of the very complex nature of the proposed emission process from cold electrodes and the uncertainty of the various influencing factors, no complete theory is known to the present authors for predicting the conditions necessary for emission. Also, the experimental data given herein are too meager and scattered to formulate as yet an empirical relationship. However, the present tests do indicate certain trends as shown by the magnitude of the apparent voltage intercept (V_S) as $I \longrightarrow 0$ (Figs. 17 through 20). The voltage required to start a high-current discharge increases as the plasma enthalpy level and/or seeding rate decrease (that is, as the free electron density decreases). These factors are most probably associated with the conditions necessary to produce short arcs across the low conductivity boundary layers to the conducting core of the plasma stream. The type of seed and pressure level appear to have important effects on V_S, but are not well documented by these experiments. Clearly much more work is needed before the physics of discharges across supersonic plasmas is fully understood.

SECTION VI
CONCLUSIONS

As part of a development program of a steady-flow, d-c, MHD accelerator, some characteristics of a d-c electrical discharge transversing a supersonic seeded nitrogen plasma have been determined. Discharges with current densities up to 100 amp/cm^2 could be achieved on each of five or six pairs of smooth, segmented, cold-copper electrodes at pressure levels between 0.3 and 1 atm, for plasma temperatures from about 2500 to 3500°K, and for potassium or NaK seeding rates from 0.2 to 2.0 percent by weight. The discharge gave the appearance of small arcs spanning the colder boundary layers on the anodes and cathodes but became diffuse in the plasma stream. The influence of (1) the plasma energy level, (2) the pressure level, (3) the seeding rate, (4) the type of seed, and (5) a magnetic field on the discharge has been documented over the limited

ranges covered by this study. The discharge was not self-sustaining, and currents ceased to flow when the seed injection was stopped. Additionally, it appeared to be most significantly affected by variations in pressure and enthalpy. Further, the discharge was found to have large current fluctuations at frequencies of 100 to 300 cps. These fluctuations were distributed in a gaussian manner about the d-c level. There is some reason to believe that the fluctuations are due to some phenomena in the boundary layers.

Water-cooled copper electrodes were found to carry large currents with negligible erosion at surface temperatures of less than 600°K.

The present tests suggest the following overall model for d-c discharges from cold electrodes transverse to a supersonic seeded plasma: (1) Field emission only slightly augmented by local thermionic emission seems to be the most probable mechanism by which the cold-copper electrodes supply electrons into the plasma. (2) Short arcs are created to span the cooler low conductivity boundary layers. (3) The plasma core, being a reasonable conductor, carries a diffuse current and has a nonequilibrium elevated electron temperature. The voltage-current characteristics of the plasma core can be roughly predicted by the Two-Temperature Conduction Law proposed by Kerrebrock (if the electron-neutral energy exchange coefficient has a value of about 100).

The present results do not completely document the characteristics of d-c discharges in seeded plasmas. Much work is still needed in order to fully understand the phenomena which occur.

REFERENCES

1. Loeb, L. B. Fundamental Processes of Electrical Discharges in Gases. John Wiley and Sons, Inc., New York, 1939.
2. Cobine, James D. Gaseous Conductors. Dover Publications, Inc., New York, 1959.
3. Bade, W. L., et al. "Theoretical and Experimental Investigation of Arc Plasma-Generation Technology." Vols. I and II, AVCO Corporation, ASD-TDR-62-729, September 1963.
4. Harris, L. P. "Electrical Conductivity of Cesium-Seeded Atmospheric Pressure Plasma near Thermal Equilibrium." Journal of Applied Physics, Vol. 34, No. 10, October 1963, p. 2958.

5. Lapp, M. and Rich, J. A. "Electrical Conductivity of Seeded Flame Plasmas in Strong Electric Fields." The Physics of Fluids, Vol. 6, No. 6, June 1963, p. 806.

6. Moore, George E. "Experimental Studies of Some Electrical Properties of Seeded Flame Plasma." ARS Ions in Flames and Rocket Exhausts Conference, October 10-12, 1962.

7. Lin, Shao-Chi, Resler, E. L., and Kantrowitz, A. "Electrical Conductivity of Highly Ionized Argon Produced by Shock Waves." Journal of Applied Physics, Vol. 26, No. 1, January 1955, p. 95.

8. Fay, J. A. and Hogan, W. T. "Heat Transfer to Cold Electrodes in a Flowing Ionized Gas." The Physics of Fluids, Vol. 5, No. 8, August 1962, p. 885.

9. Smy, P. R. and Driver, H. S. "Electrical Conductivity of Low-Pressure Shock-Ionized Argon." Journal of Fluid Mechanics, Vol. 17, Part 2, October 1963, p. 182.

10. Smy, P. R. "Electrical Impedance of Electrodes Immersed in Moving Plasma." Canadian Journal of Physics, Vol. 41, August 1963, p. 1346-1358.

11. Marlotte, Gary L. "An Experimental Investigation of the Effect of a Transverse Hypersonic Flow Velocity upon a Low-Density D. C. Electrical Discharge in Air." Firestone Flight Sciences Laboratory, California Institute of Technology, Memorandum No. 66, June 1962.

12. Thiene, Paul G., et al. "An Experimental Investigation of the Behavior of an Arc Positive Column in the Presence of Forced Convection." Plasmadyne Corp., Santa Ana, California, AFOSR 682, April 1961.

13. Thiene, Paul. "Convective Flexure of a Plasma Conductor." The Physics of Fluids, Vol. 6, No. 9, September 1963, p. 1319.

14. "Proceedings of Second Symposium on the Engineering Aspects of Magnetohydrodynamics." University of Pennsylvania, March 9-10, 1961.

15. "Proceedings of Third Symposium on the Engineering Aspects of Magnetohydrodynamics." University of Rochester, Rochester, New York, March 28-29, 1962.

16. "Proceedings of Fourth Symposium on the Engineering Aspects of Magnetohydrodynamics." University of California, Berkeley, April 10-11, 1963.

17. "Proceedings of Fifth Symposium on Engineering Aspect of Magnetohydrodynamics." Massachusetts Institute of Technology, April 1-2, 1964.

18. Grey, J., et al. "Calorimetric Probe for the Measurement of Extremely High Temperatures." Review of Scientific Instruments, Vol. 33, No. 7, July 1962, p. 738.

19. Cunningham, J. W. and Dicks, J. B. "A Microwave Method of Measuring Plasma Velocity." Proceedings of the Third Hypervelocity Techniques Symposium, Denver, March 1964.

20. Demetriades, S. T. and Ziemer, R. W. "Three-Fluid Non-Equilibrium Plasma Accelerators." Electric Propulsion Conference, Paper 2375-62, March 14-16, 1962.

21. Denison, M. Richard and Ziemer, Richard W. "Investigation of the Phenomena in Cross-Field Plasma Accelerators." Presented at the Fifth Biennial Gas Dynamics Symposium, Northwestern University, Paper No. 63-378, August 14-16, 1963.

22. Dimmock, T. Herbert and Kineyko, William R. "Ionization Profiles in Low Pressure Exhausts." Presented at 5th Biennial Gas Dynamic Symposium, Northwestern University, August 14-16, 1963, AIAA Preprint 63-388.

23. Weber, R. E. and Tempelmeyer, K. E. "Calculation of the D-C Electrical Conductivity of Equilibrium Nitrogen and Argon Plasma with and without Alkali Metal Seed." AEDC-TDR-64-119 (AD 602858), May 1964.

24. Kerrebrock, Jack L. "Conduction in Gases with Elevated Electron Temperature." Proceedings of the Second Symposium on the Engineering Aspects of Magnetohydrodynamics, University of Pennsylvania, March 9-10, 1961.

25. Kerrebrock, J. L. and Hoffman, M. A. "Experiments on Non-Equilibrium Ionization Due to Electron Heating." Presented at the 1964 AIAA Aerospace Sciences Meeting, New York, N. Y., January 20-22, 1964, Preprint No. 64-27.

26. Zukowski, E. E., Cool, T. A., and Gibson, E. G. "Experiments Concerning Non-Equilibrium Conductivity in a Seeded Plasma." Presented at the 1964 AIAA Aerospace Sciences Meeting, New York, N. Y., January 20-22, 1964, Preprint No. 64-28.

27. Spitzer, Lyman, Jr. Physics of Fully Ionized Gases. Interscience Publishers, Division of John Wiley and Sons, New York, 1962. (Second Edition, No. 3)

28. Kerrebrock, Jack L. "Nonequilibrium Ionization Due to Electron Heating: I. Theory." AIAA Journal, Vol. 2, No. 6, June 1964, pp. 1072-1080.

29. Curry, B. P. Private Communication, April 1964.

30. Gomer, Robert. Field Emission and Field Ionization. Harvard University Press, 1961.

31. Murphy, E. L. and Good, R. H. "Thermionic Emission, Field Emission, and the Transition Region." Physical Review, Vol. 102, No. 6, 1956, p. 1464-1473.

32. Jones, F. Llewellyn, and Nicholas, D. J. "Mechanism of Field Induced Emission from Cold Electrodes in Gases." Proceedings of the Fifth International Conference on Ionization Phenomena in Gases, Vol. II, August 1961.

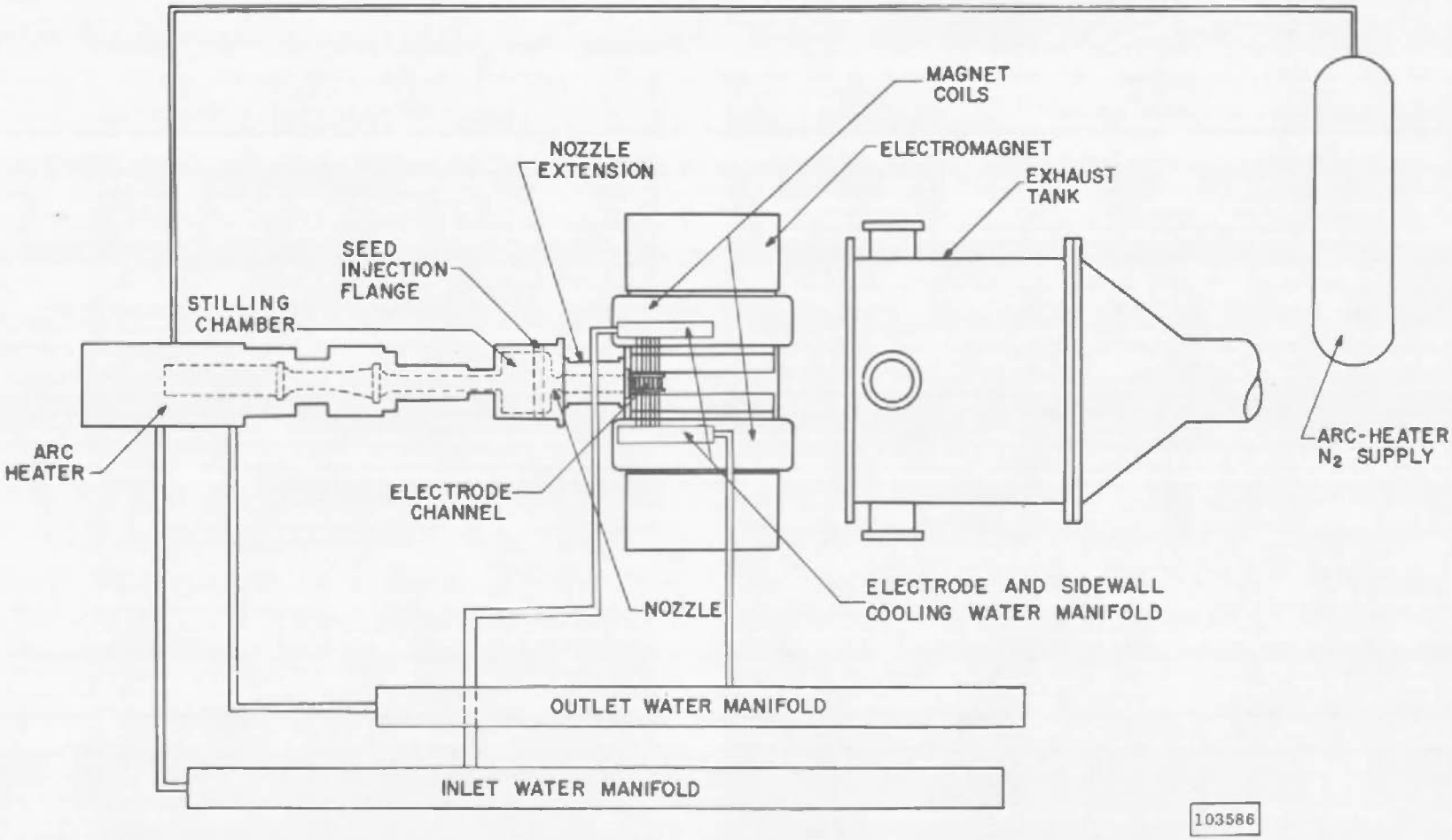

Fig. 1 Schematic of Test Apparatus

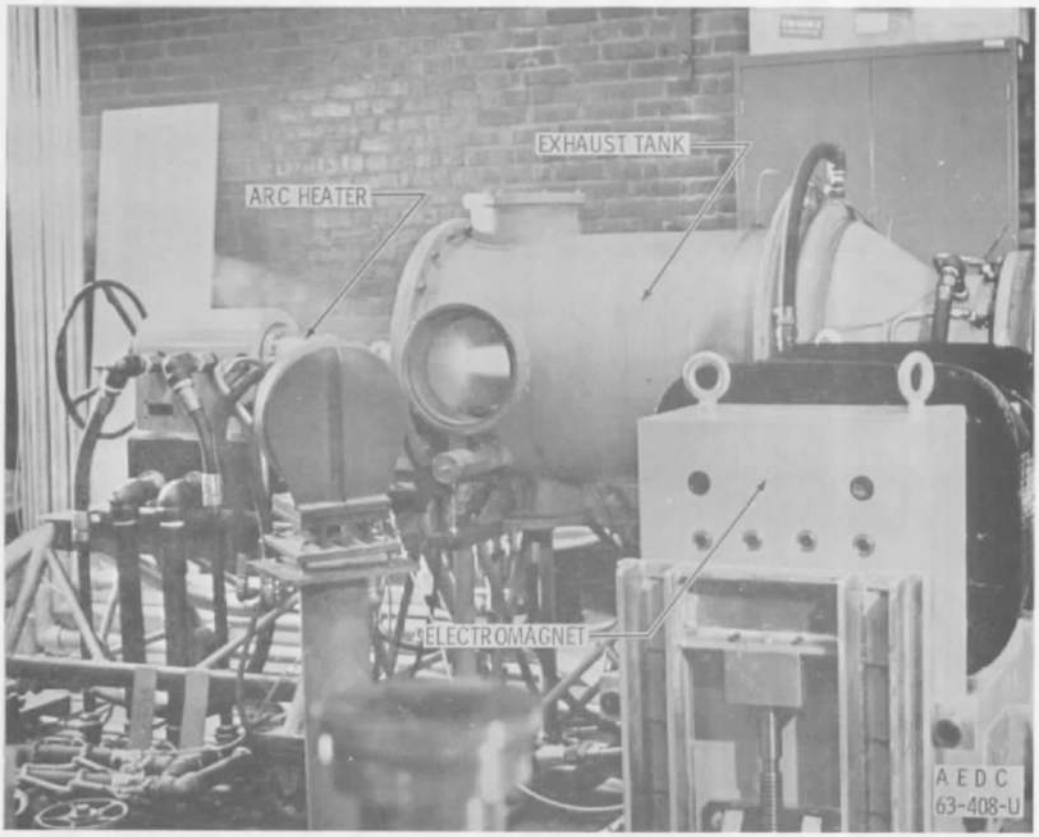

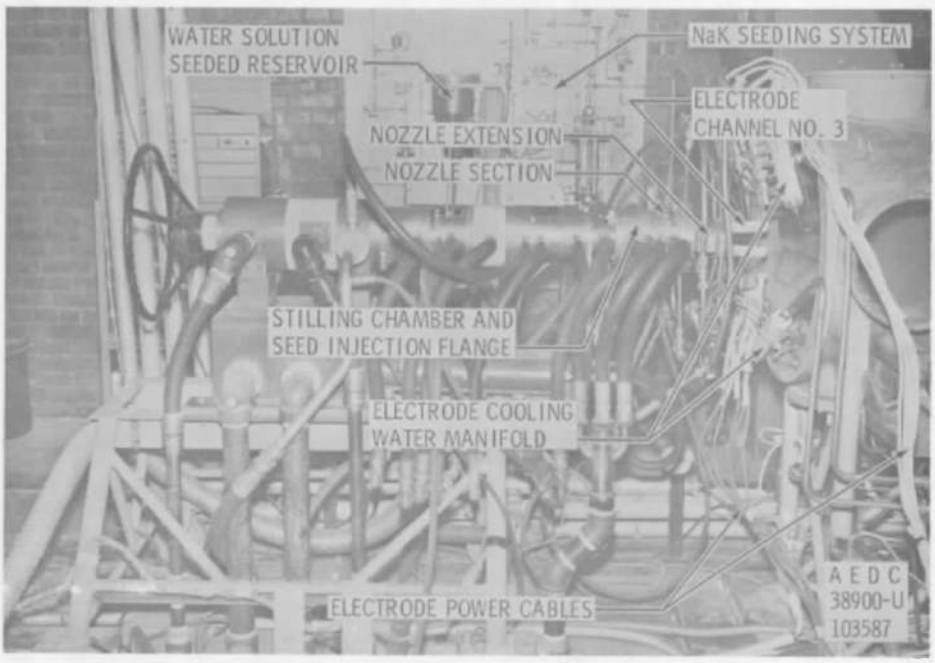

Fig. 2 Photograph of Test Equipment

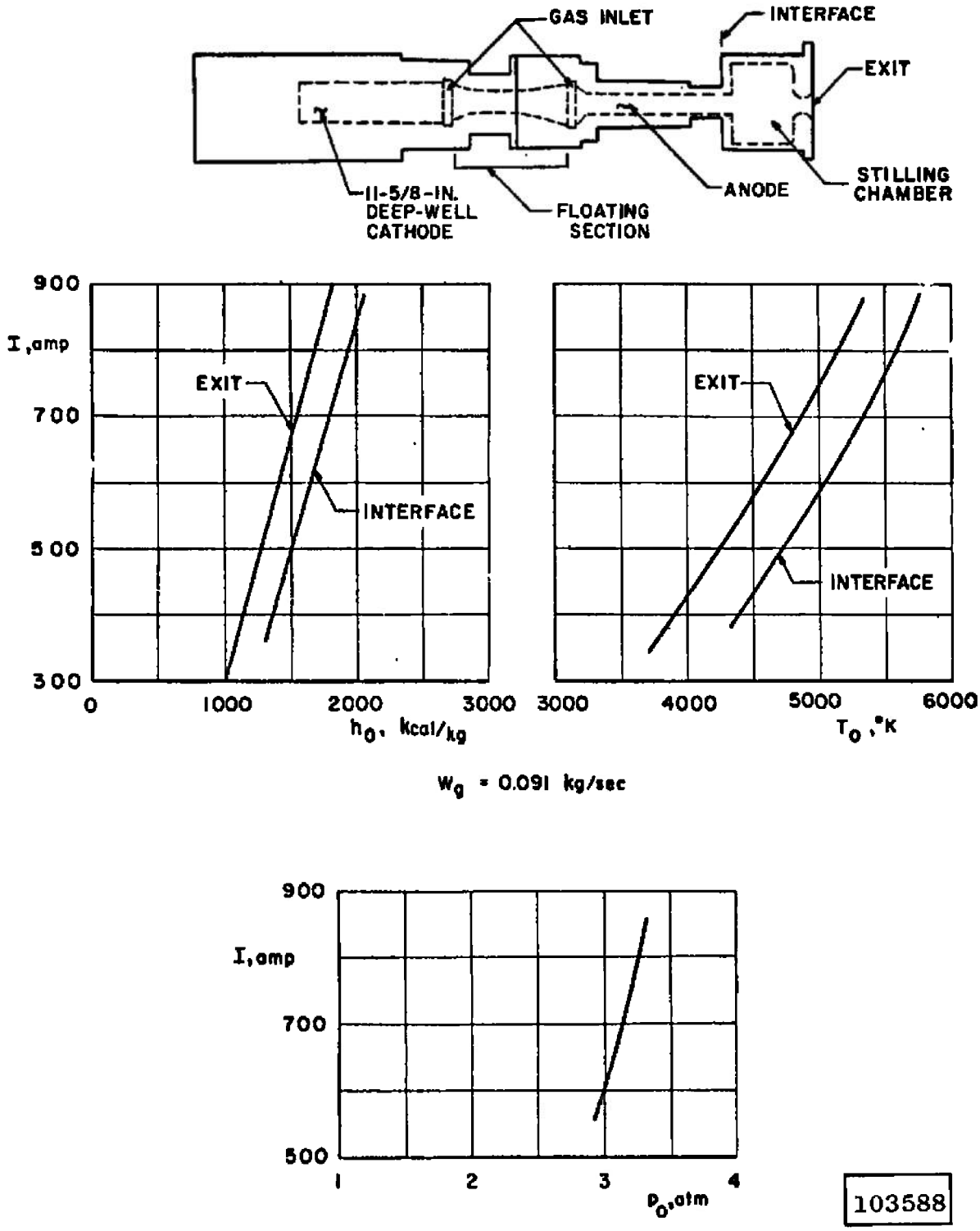

Fig. 3 Typical Arc-Heater Performance Characteristics

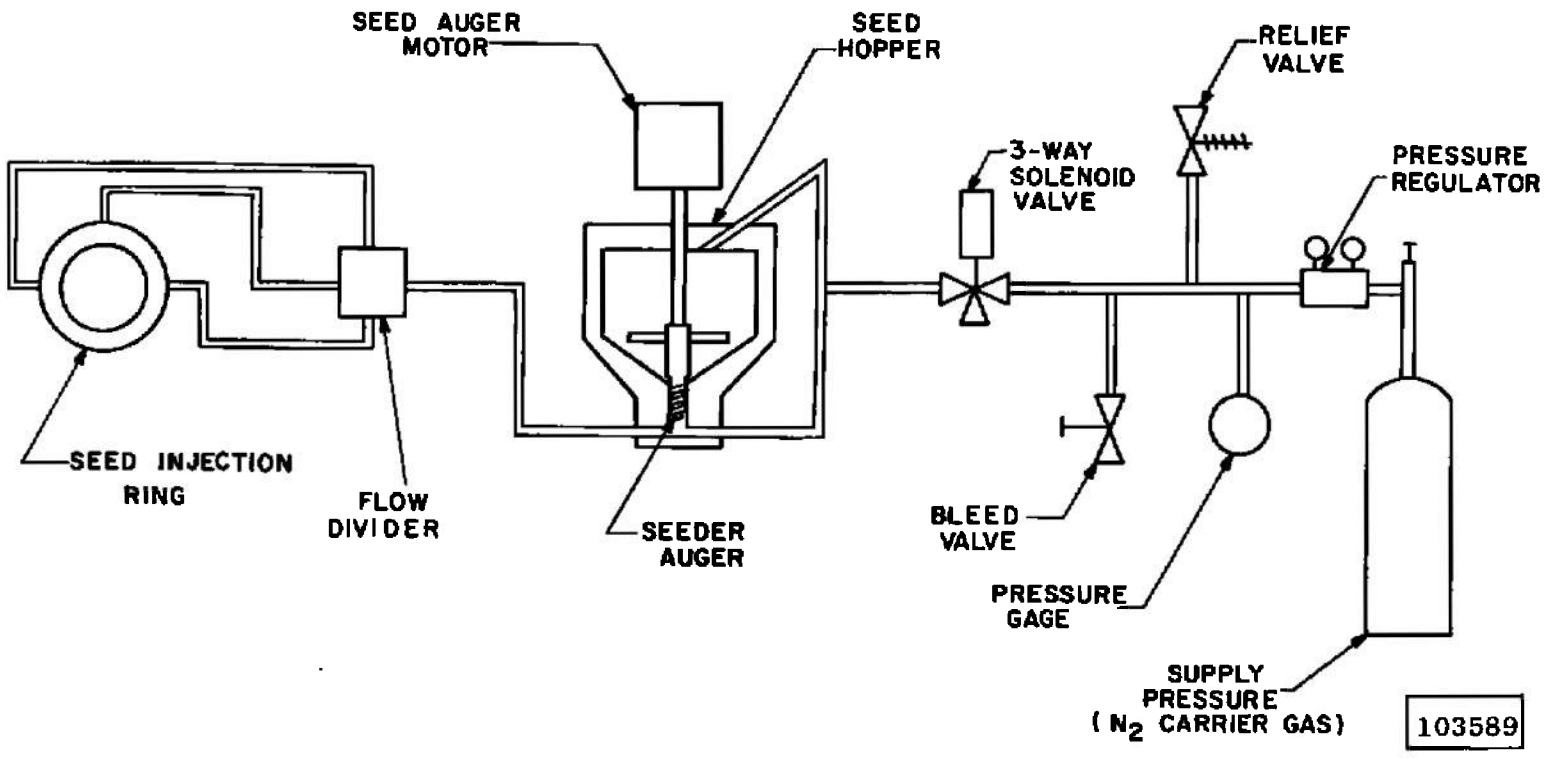

Fig. 4 Schematic of Powder Seeding System

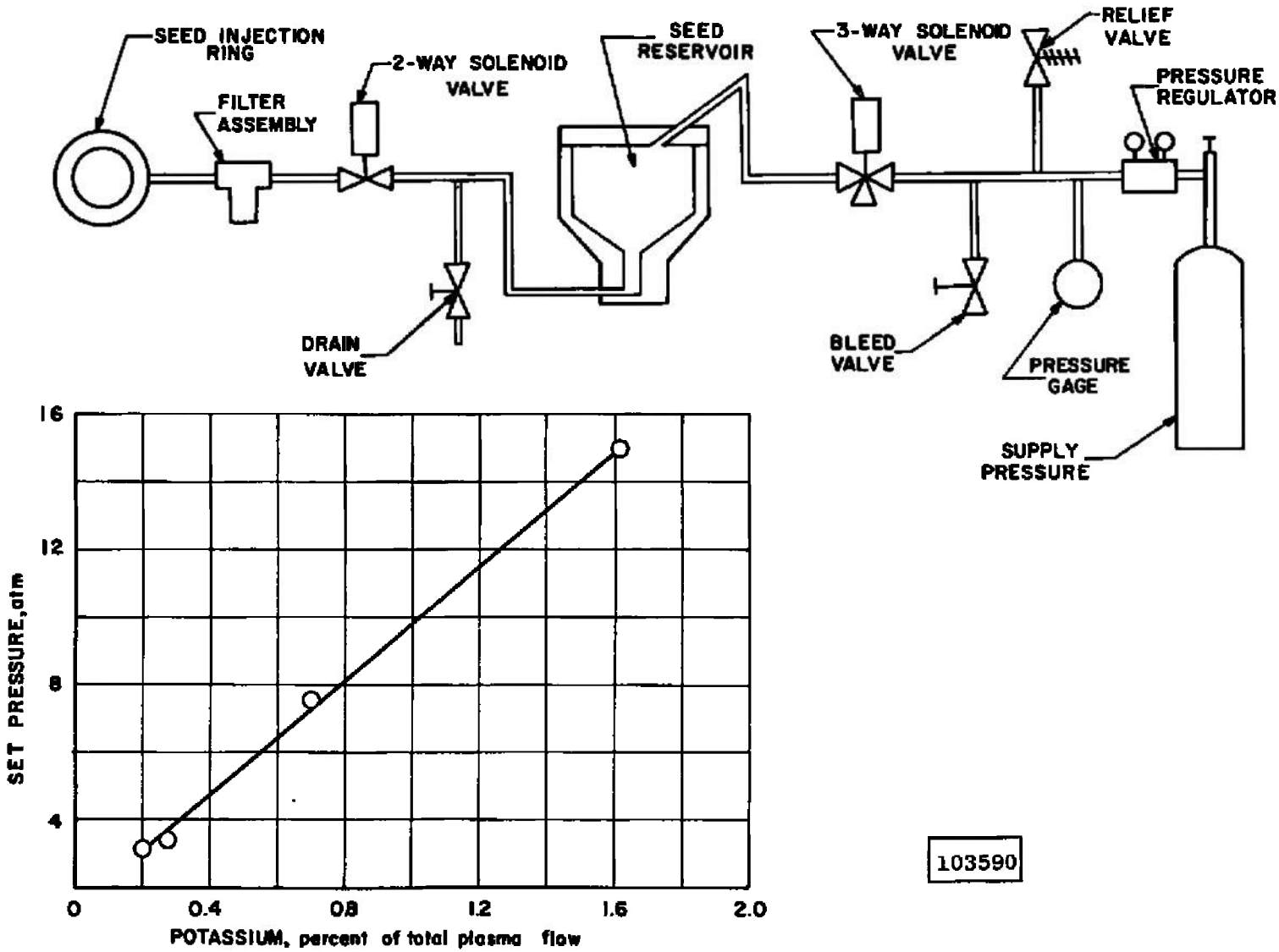

Fig. 5 Schematic of K_2CO_3 Water Solution Seeding System

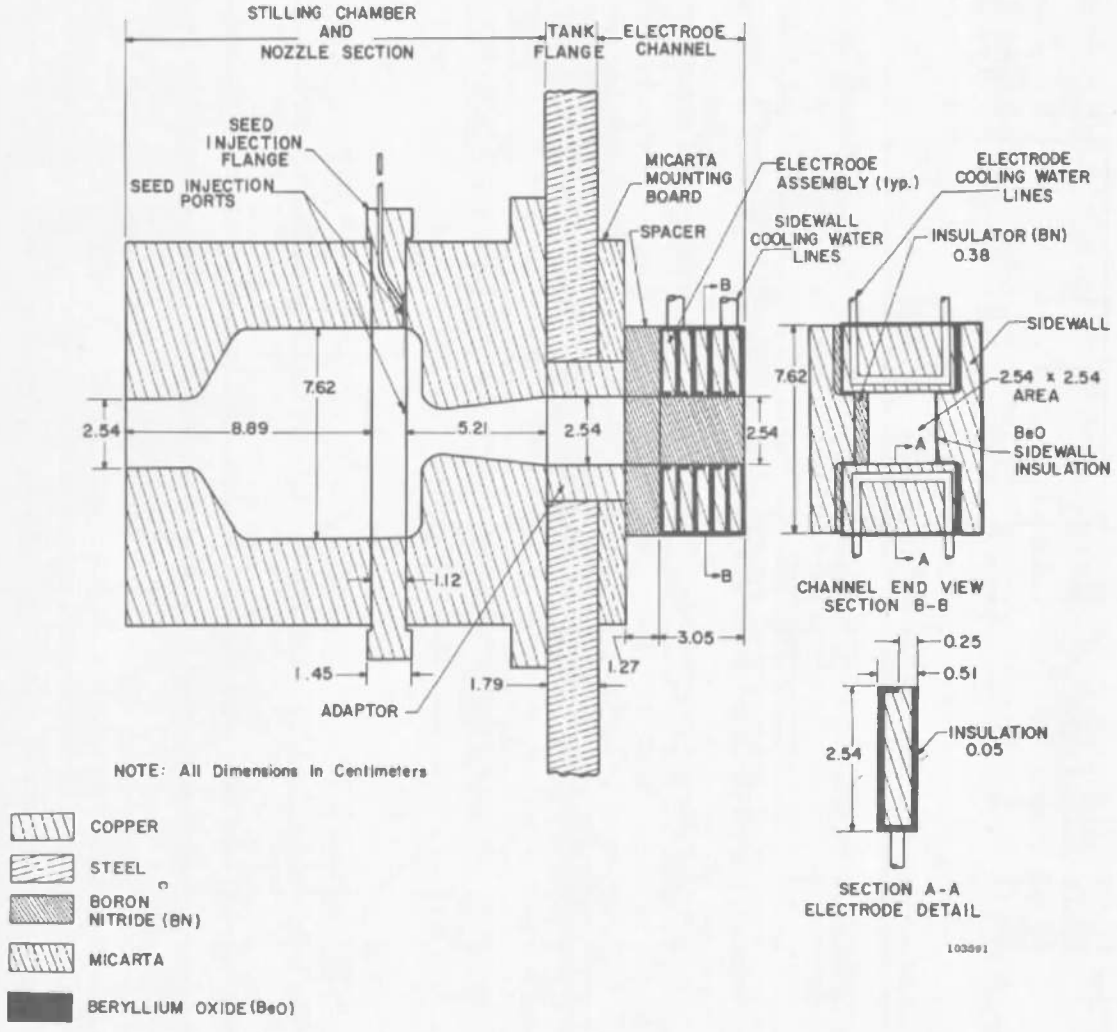

Fig. 6 Schematic of Channel 1 Mounted on the Stilling Chamber, Seeding Flange, and Nozzle Assembly

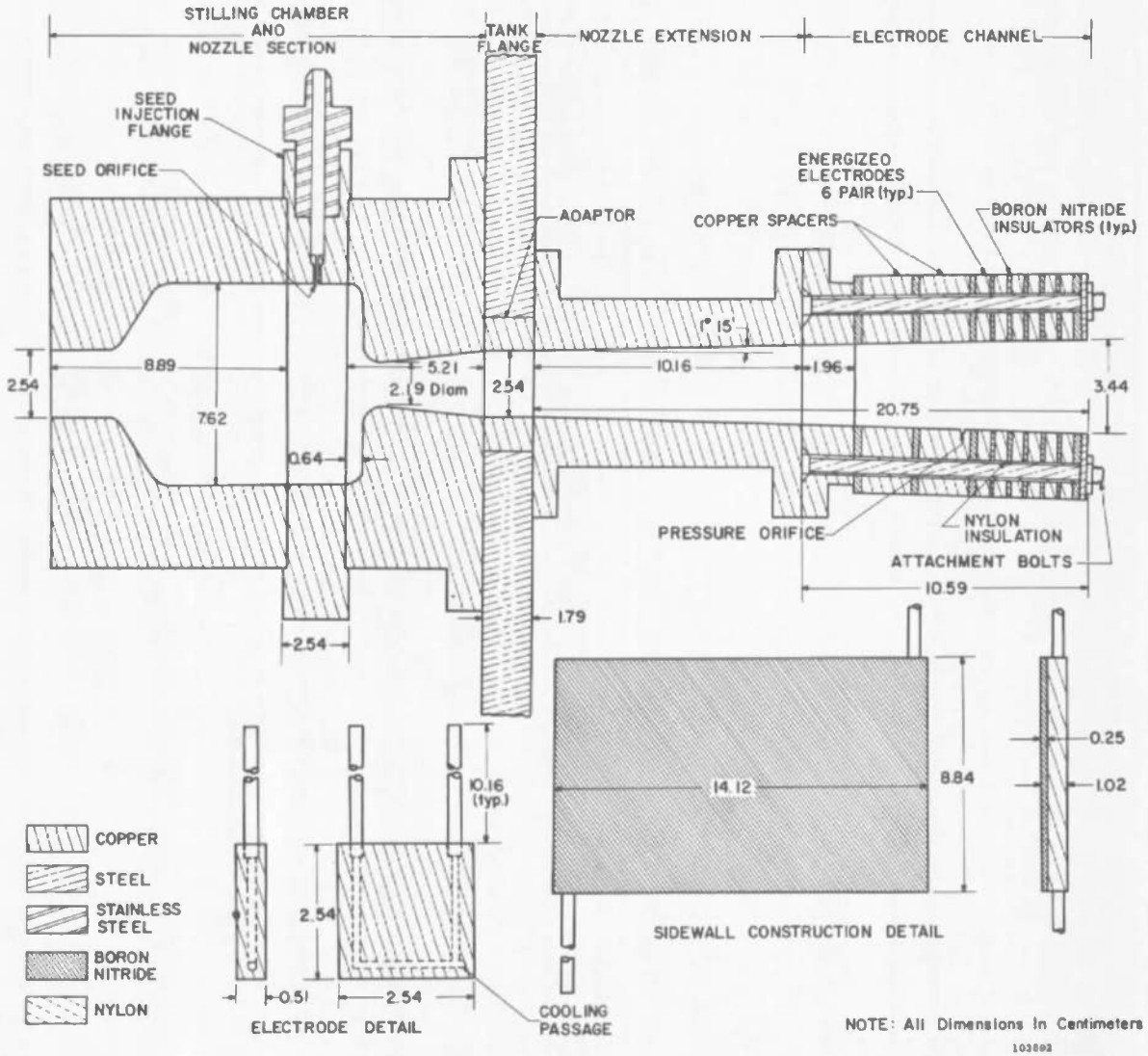

Fig. 7 Schematic of Channel 2 Mounted on the Stilling Chamber, Seeding Flange, Nozzle, and Nozzle Extension Assembly

NOTE: All Dimensions in Centimeters

ELECTRODE DETAILS - SAME AS CHANNEL 2

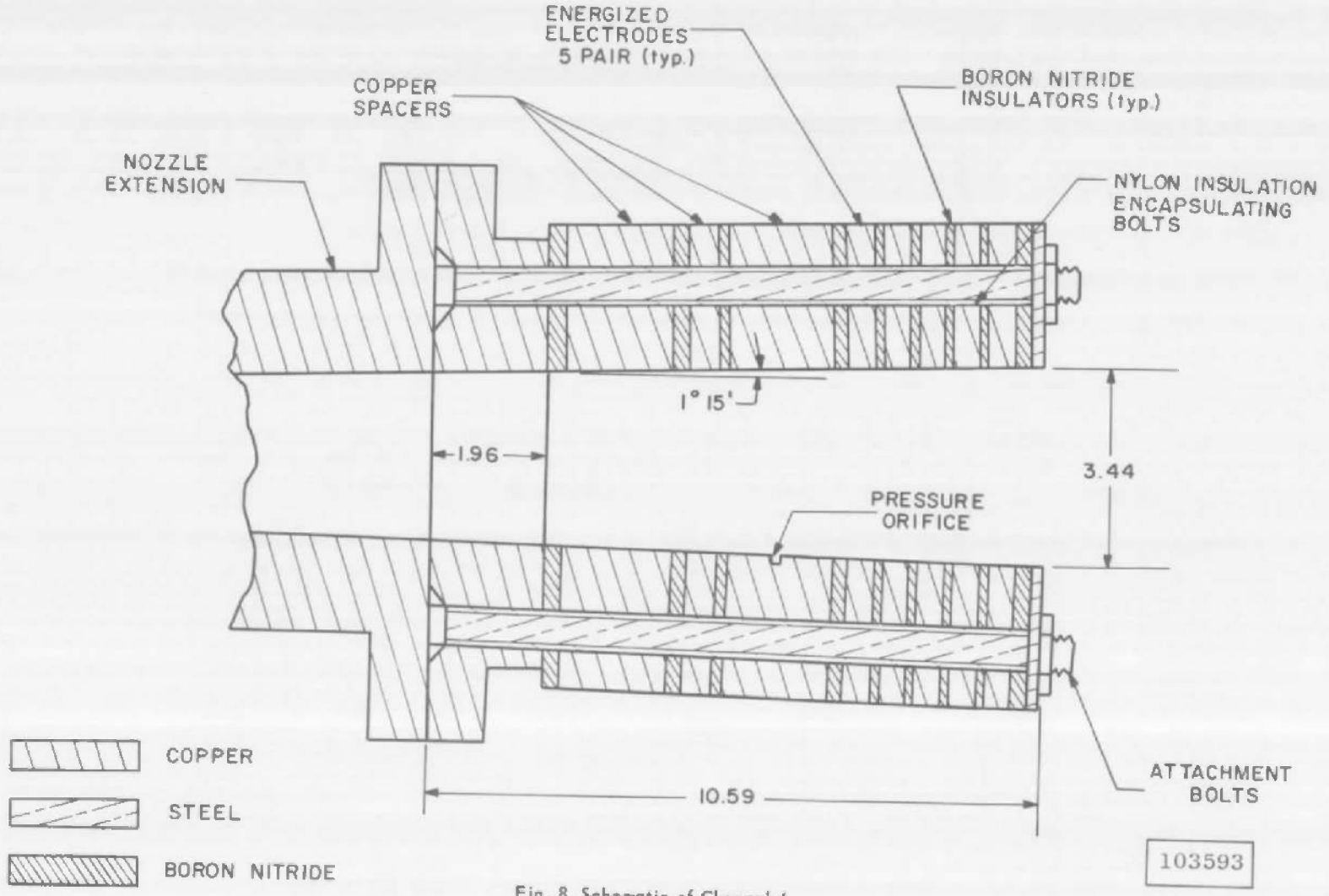

Fig. 8 Schematic of Channel 4

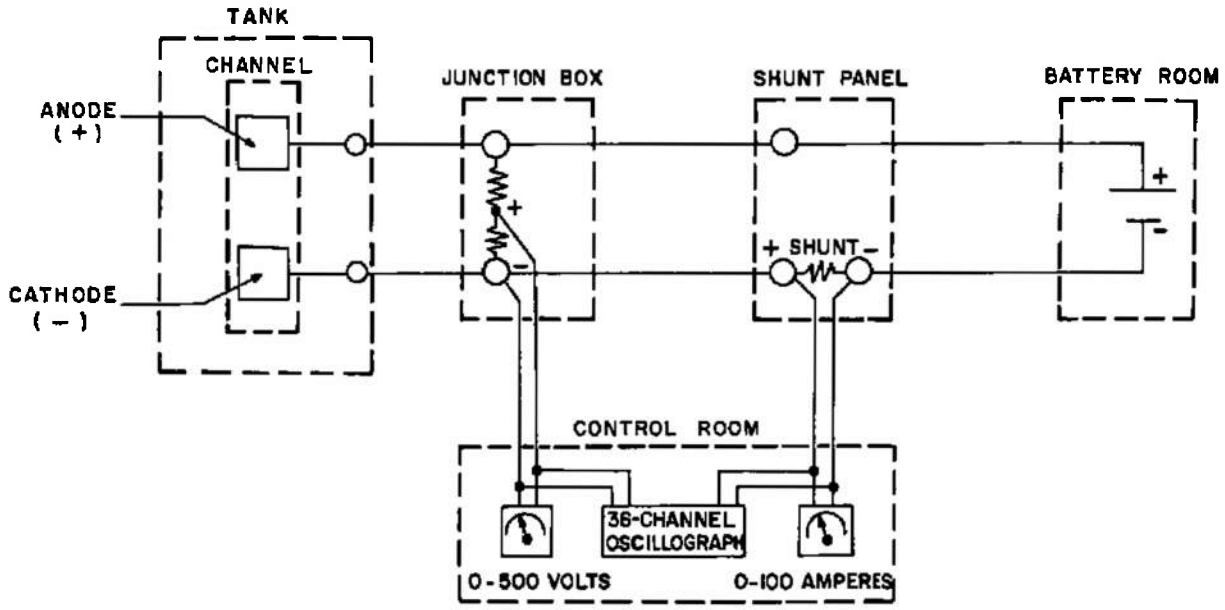

a. Electrical System Schematic

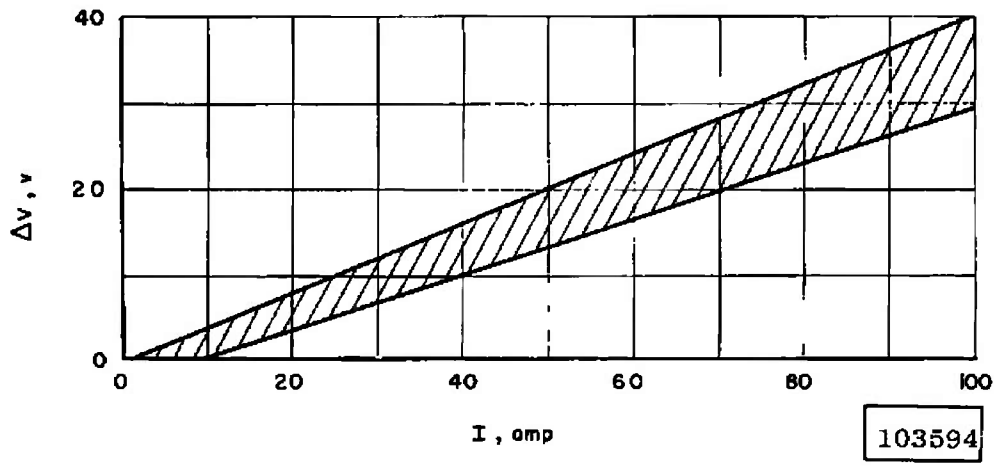

b. Battery Voltage Drop vs Load Current

Fig. 9 Electrode Electrical System Details

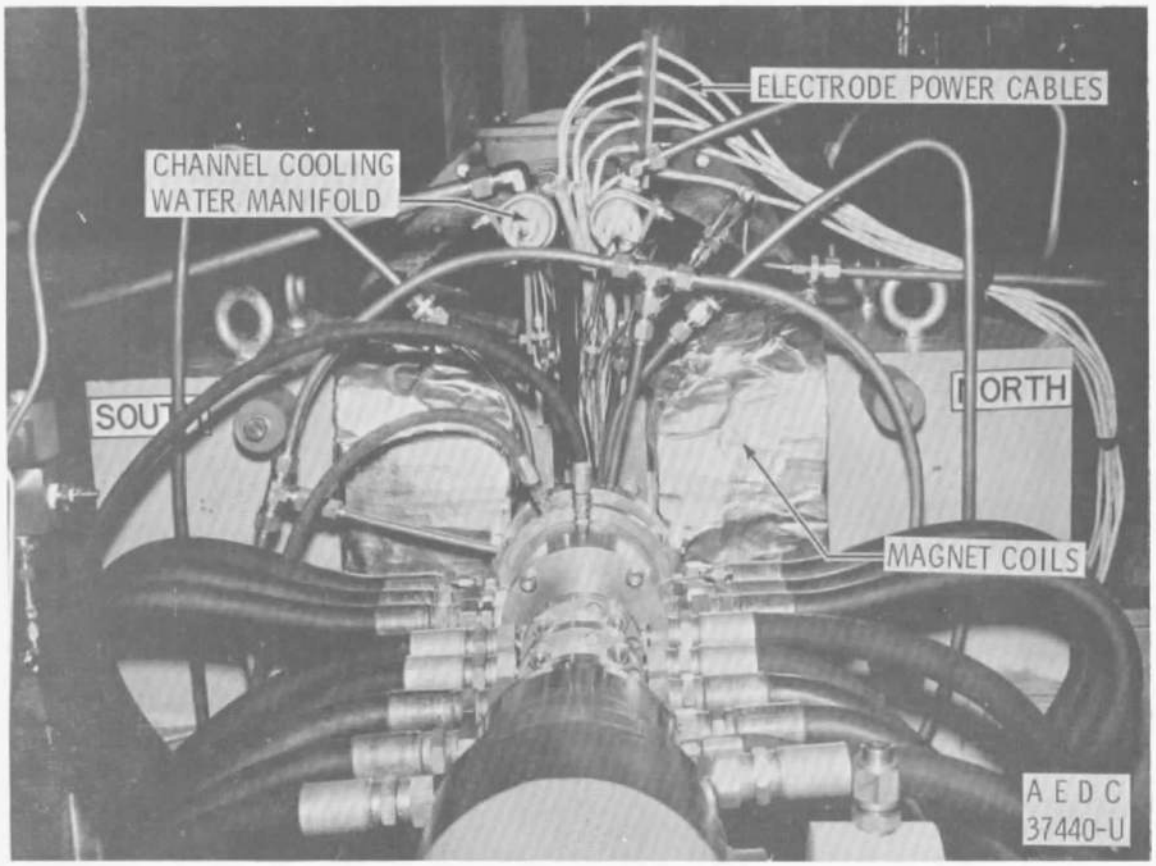

a. Photograph of Channel 2 Installed in Magnet

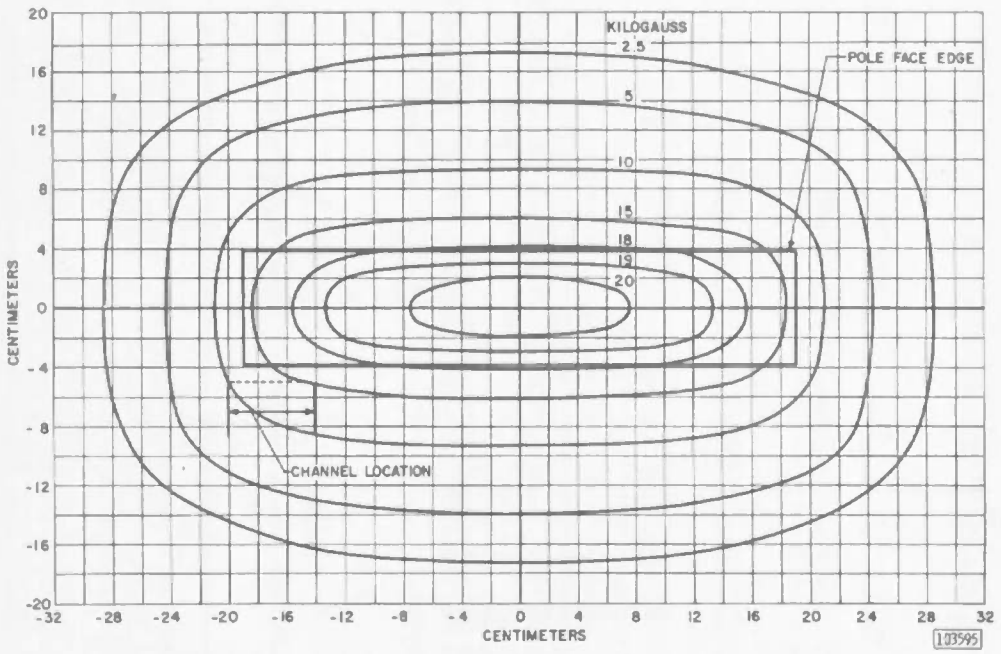

b. Magnet Field Distribution

Fig. 10 Magnet Installation Details

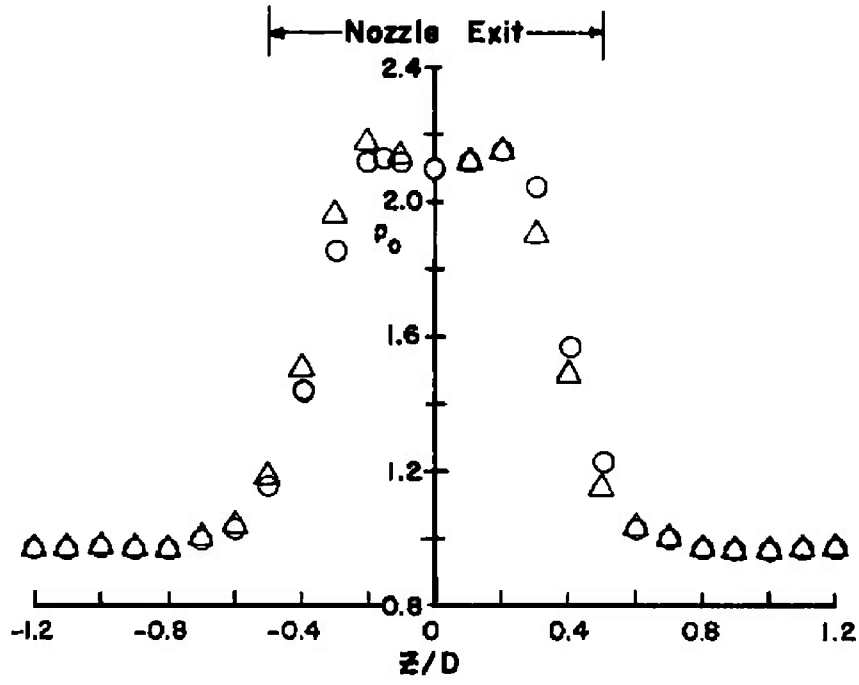

a. No Seed

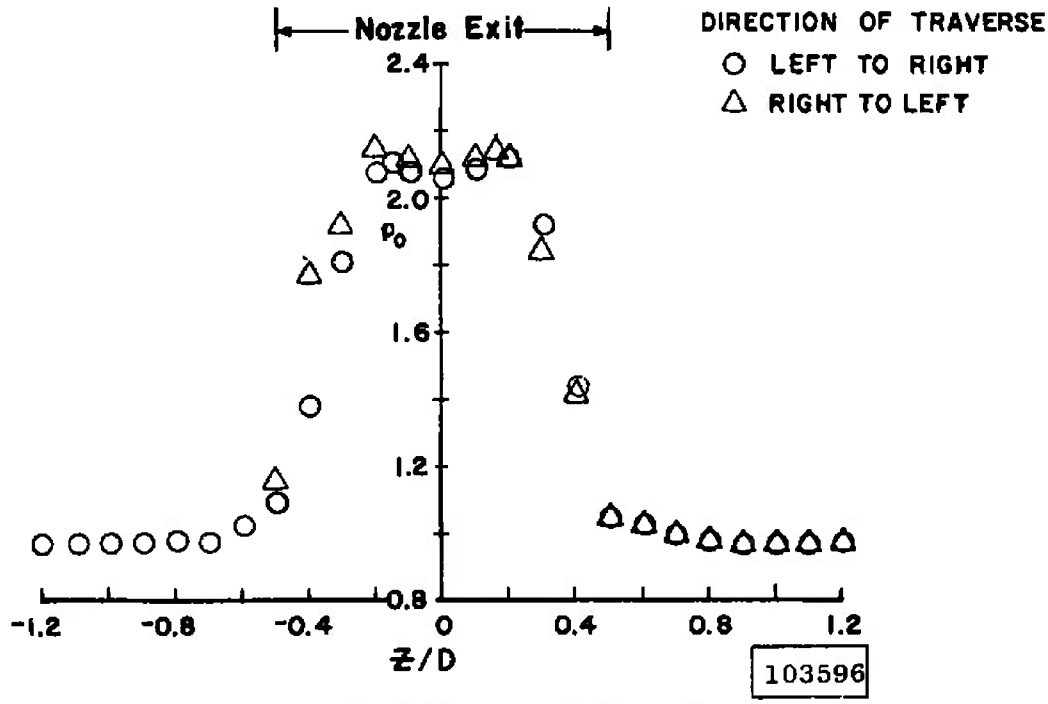

b. S = 1.135 percent (K_2CO_3 + H_2O)

Fig. 11 Typical Impact Pressure Profiles at Channel Entrance

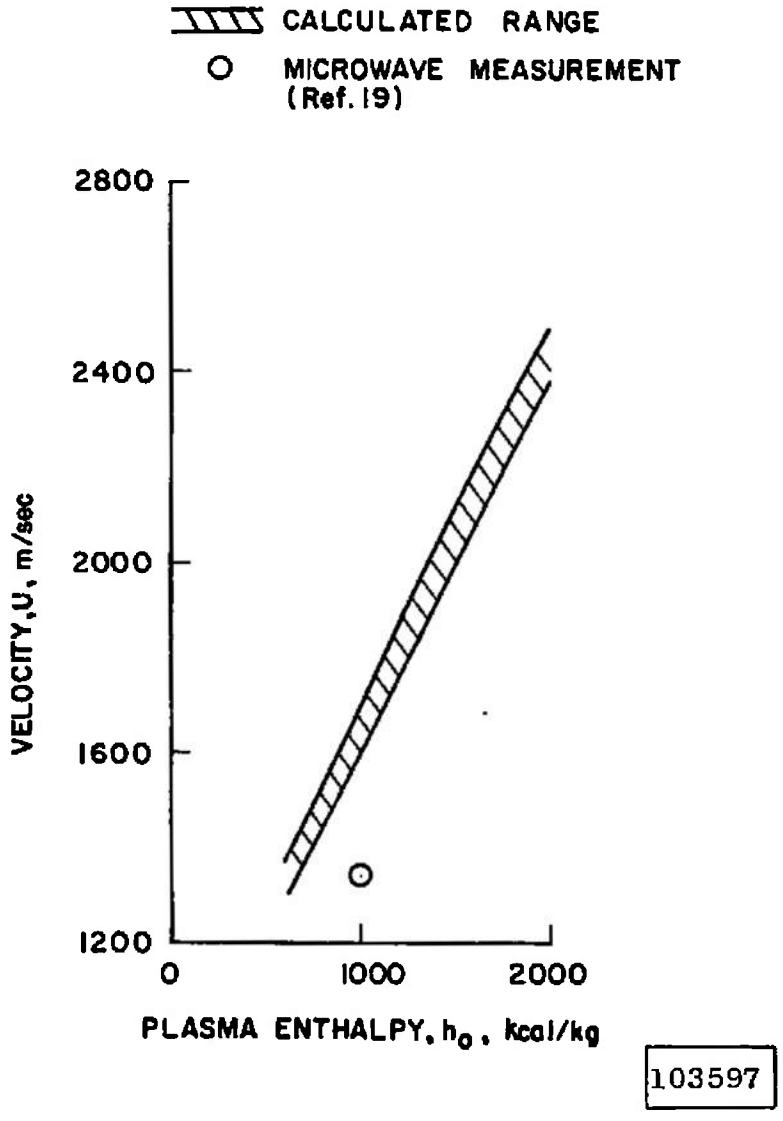

Fig. 12 Estimated Plasma Velocity at Channel Entrance

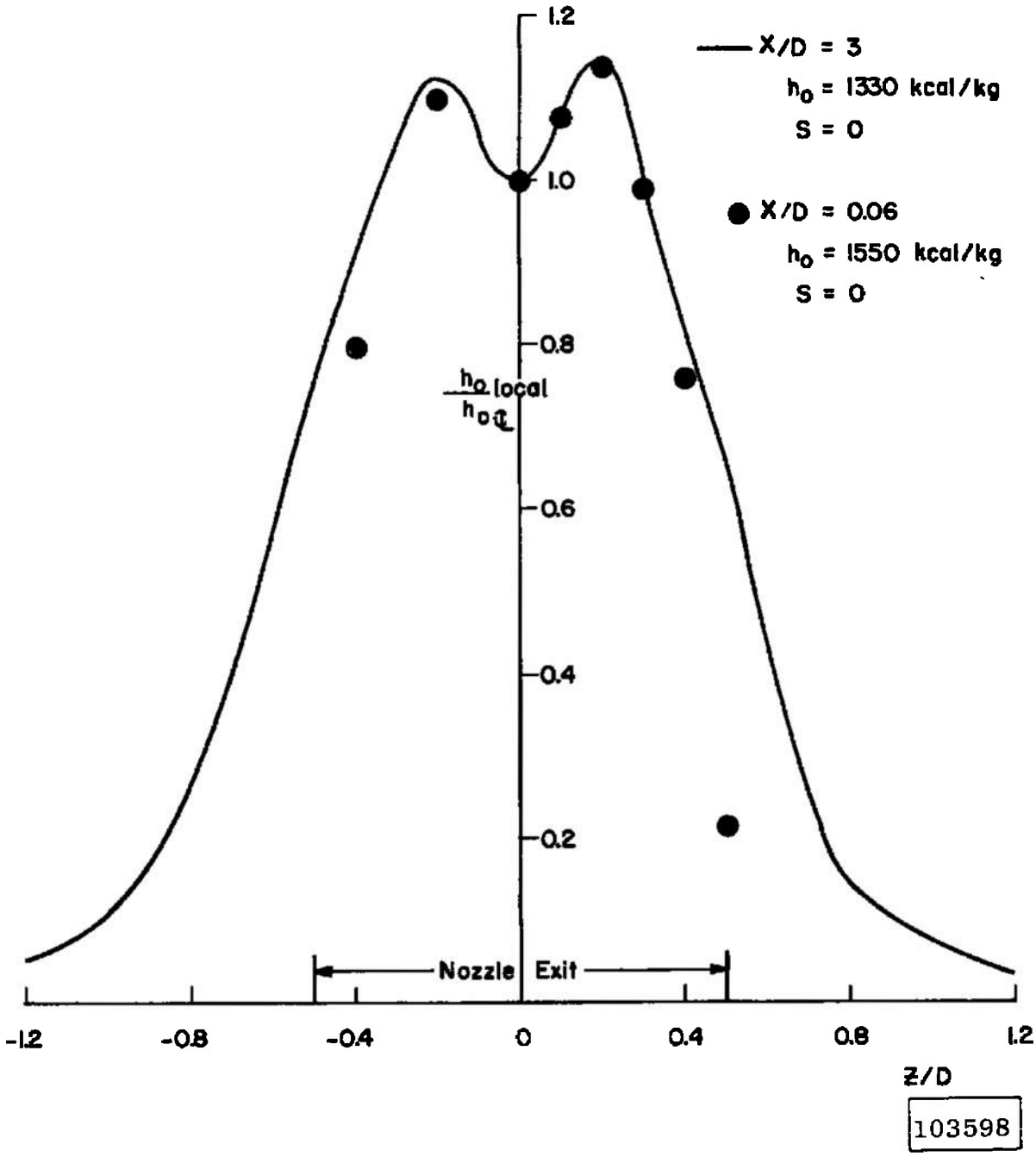

Fig. 13 Stagnation Enthalpy Profile at the Channel Entrance

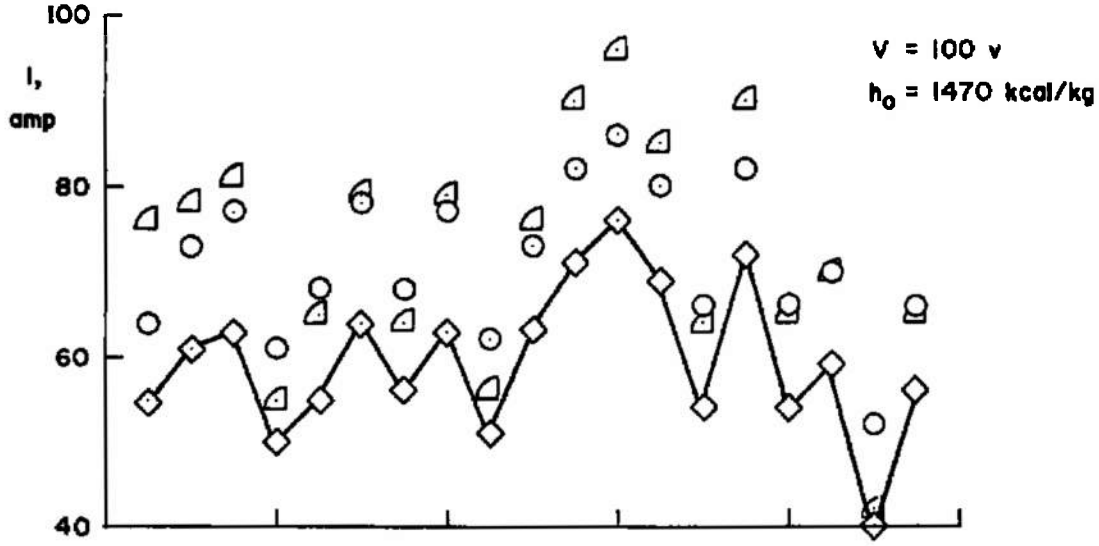

a. K_2CO_3 Powder Seed, S = 1 percent

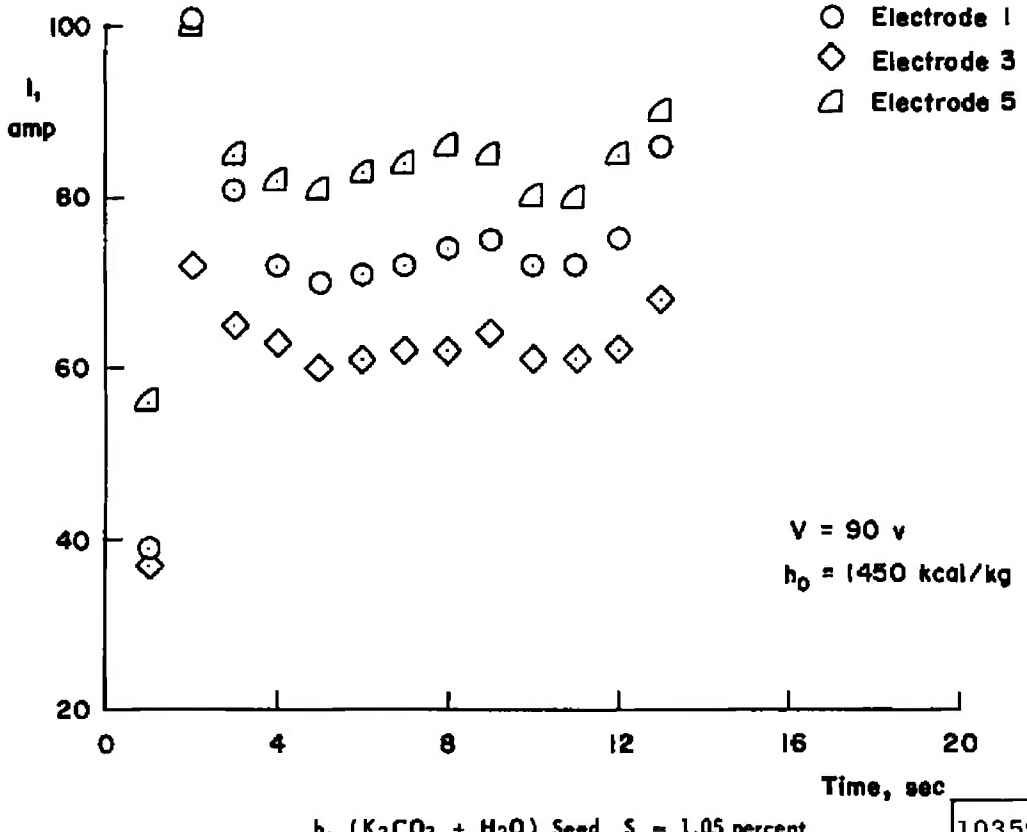

b. (K_2CO_3 + H_2O) Seed, S = 1.05 percent

103599

Fig. 14 Long-Duration Current Fluctuations for Channel 1 Operating with K_2CO_3 Seed

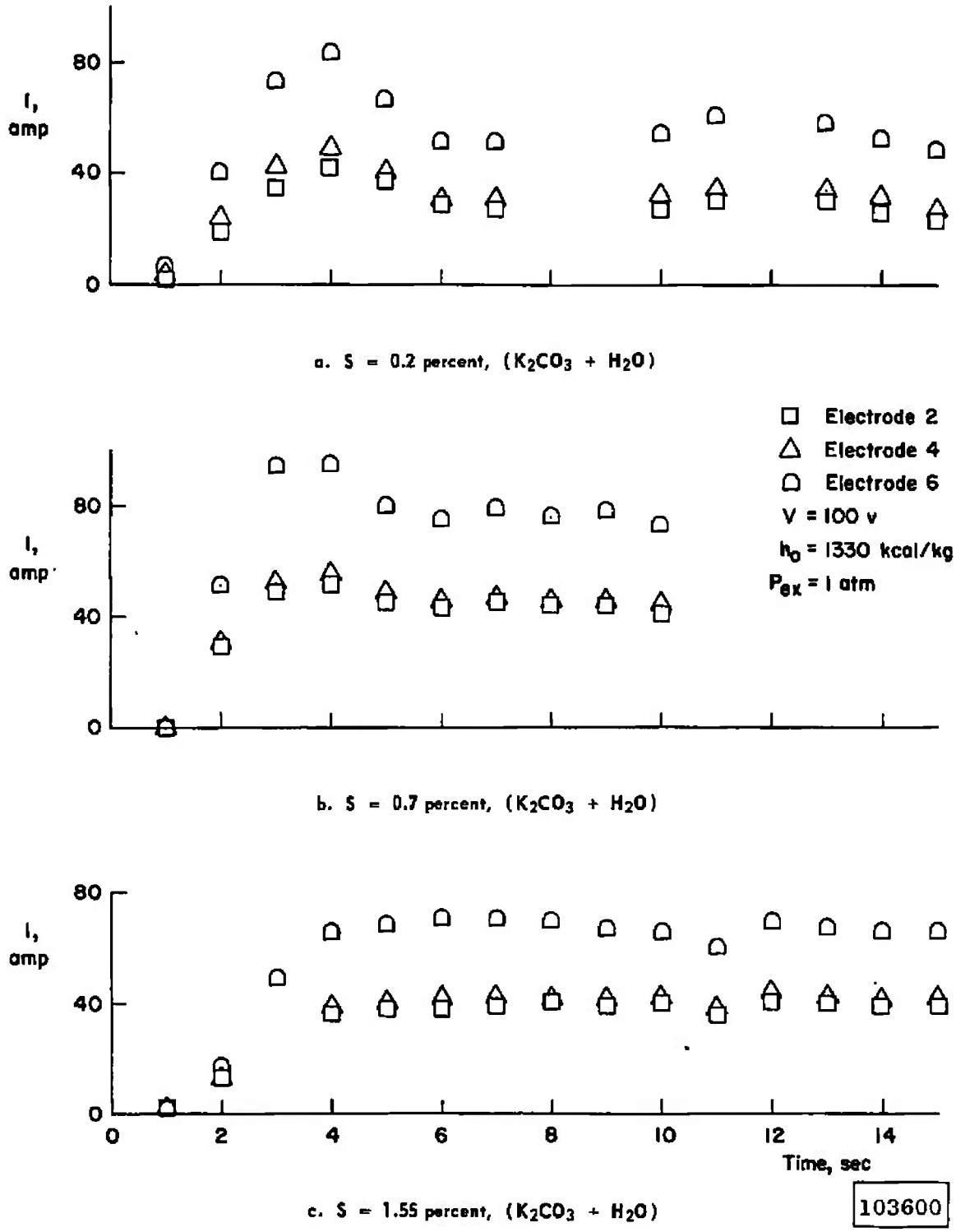

Fig. 15 Effect of Seeding Rate on Long-Duration Current Fluctuations for Channel 3

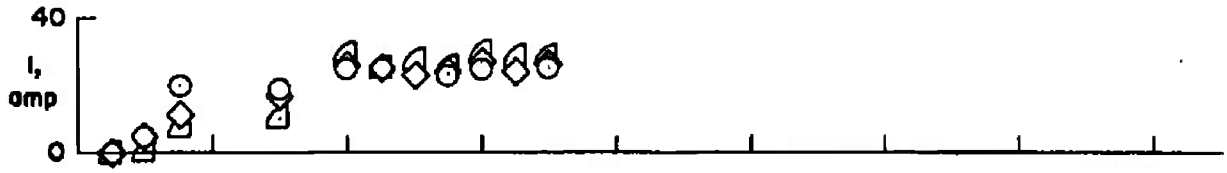

a. S = 0.5 percent, NaK Seed

b. S = 1.05 percent, NaK Seed

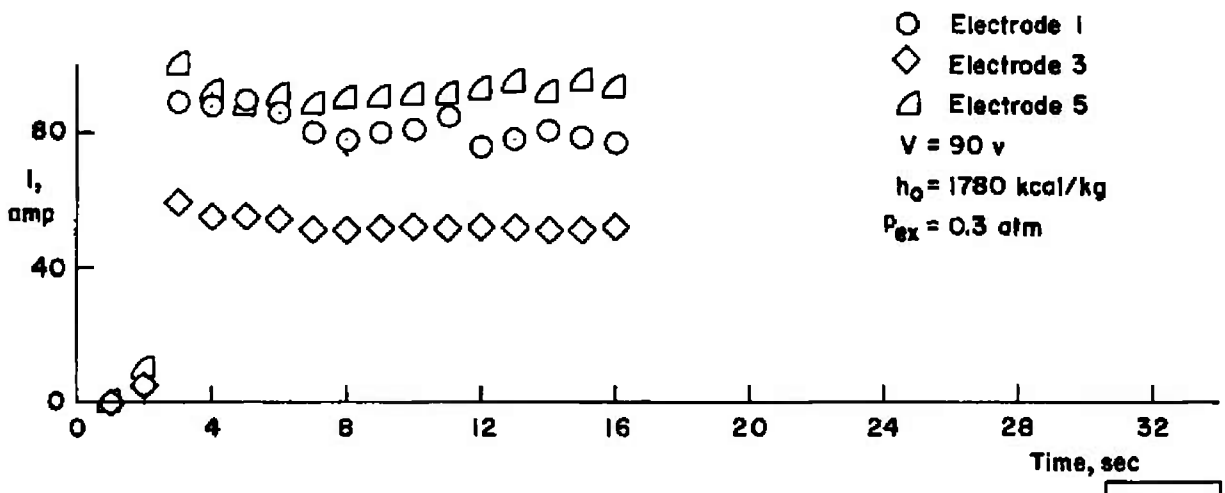

c. S = 1.9 percent, NaK Seed

Fig. 16 Long-Duration Current Fluctuations for Channel 4 Operating with NaK Seed

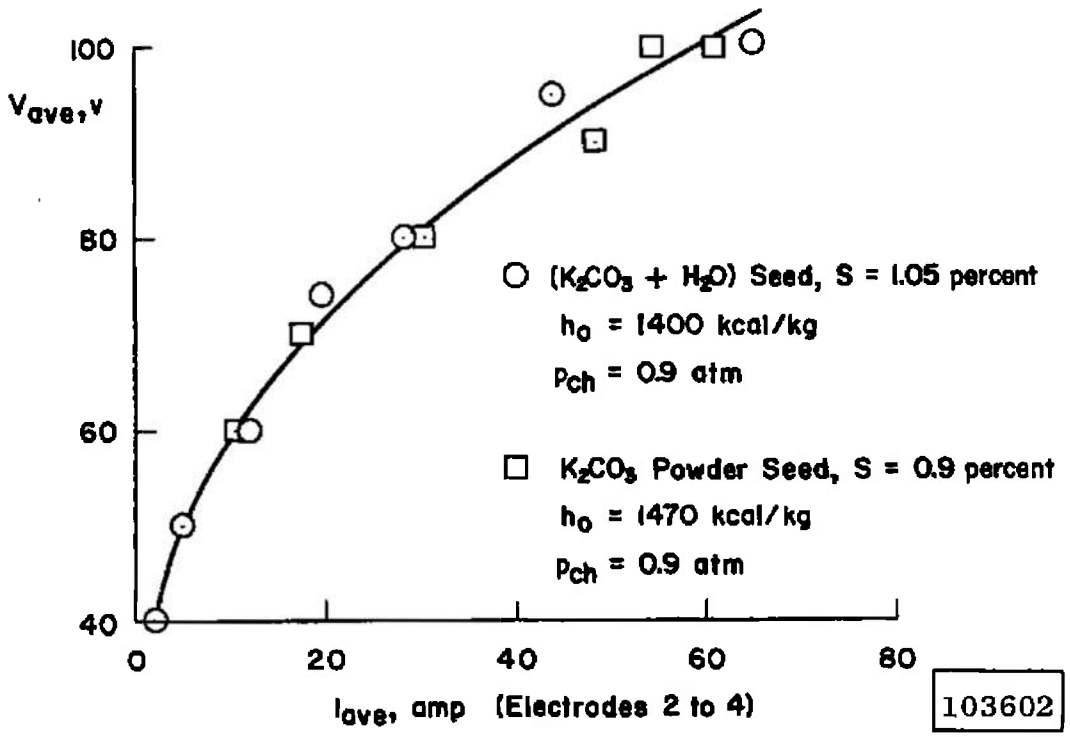

Fig. 17 Averaged Current-Voltage Characteristics for Channel 1 with Powder and Liquid K_2CO_3 Seed

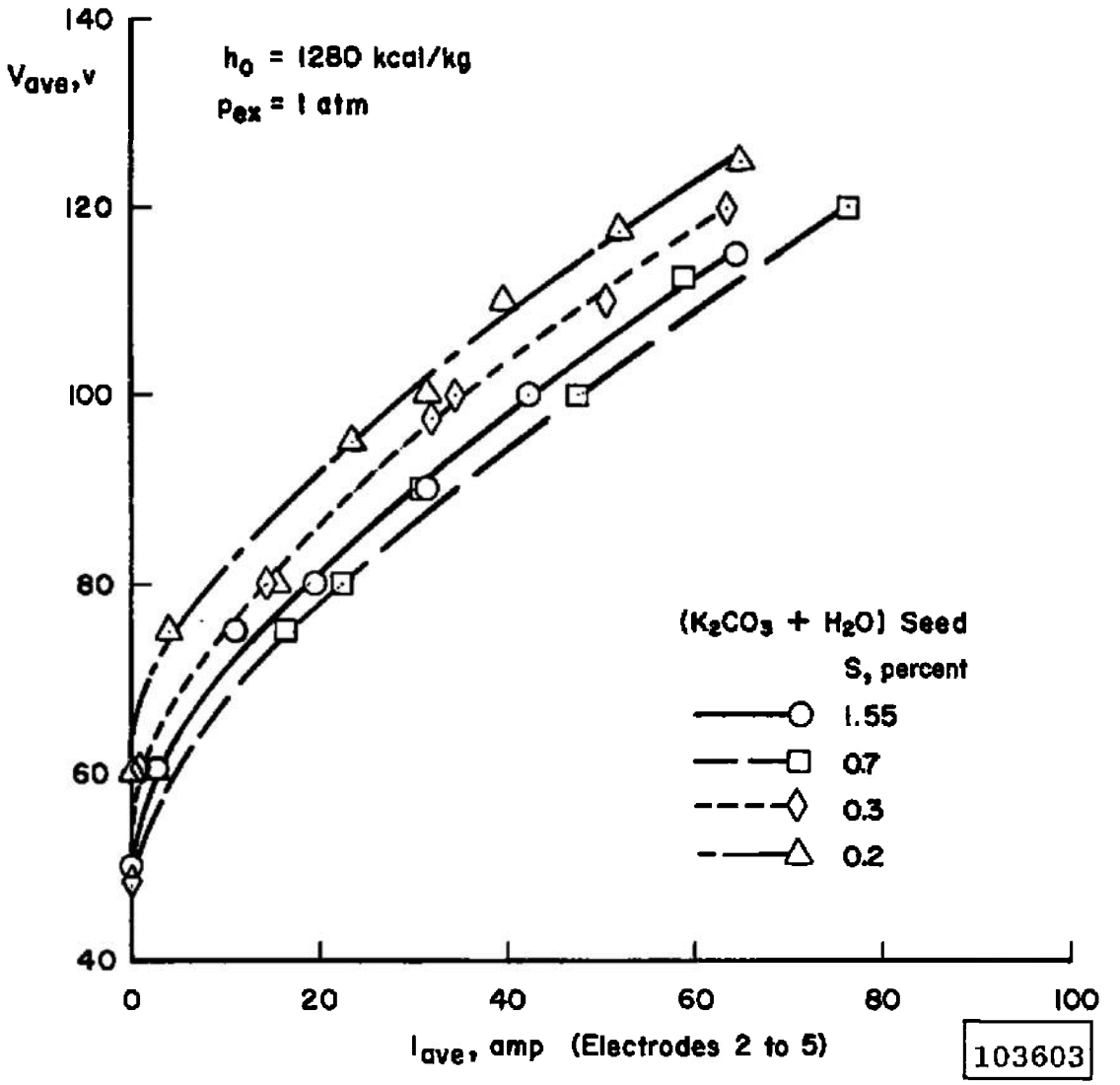

Fig. 18 Averaged Current-Voltage Characteristics for Channel 2 at Various Seed Rates

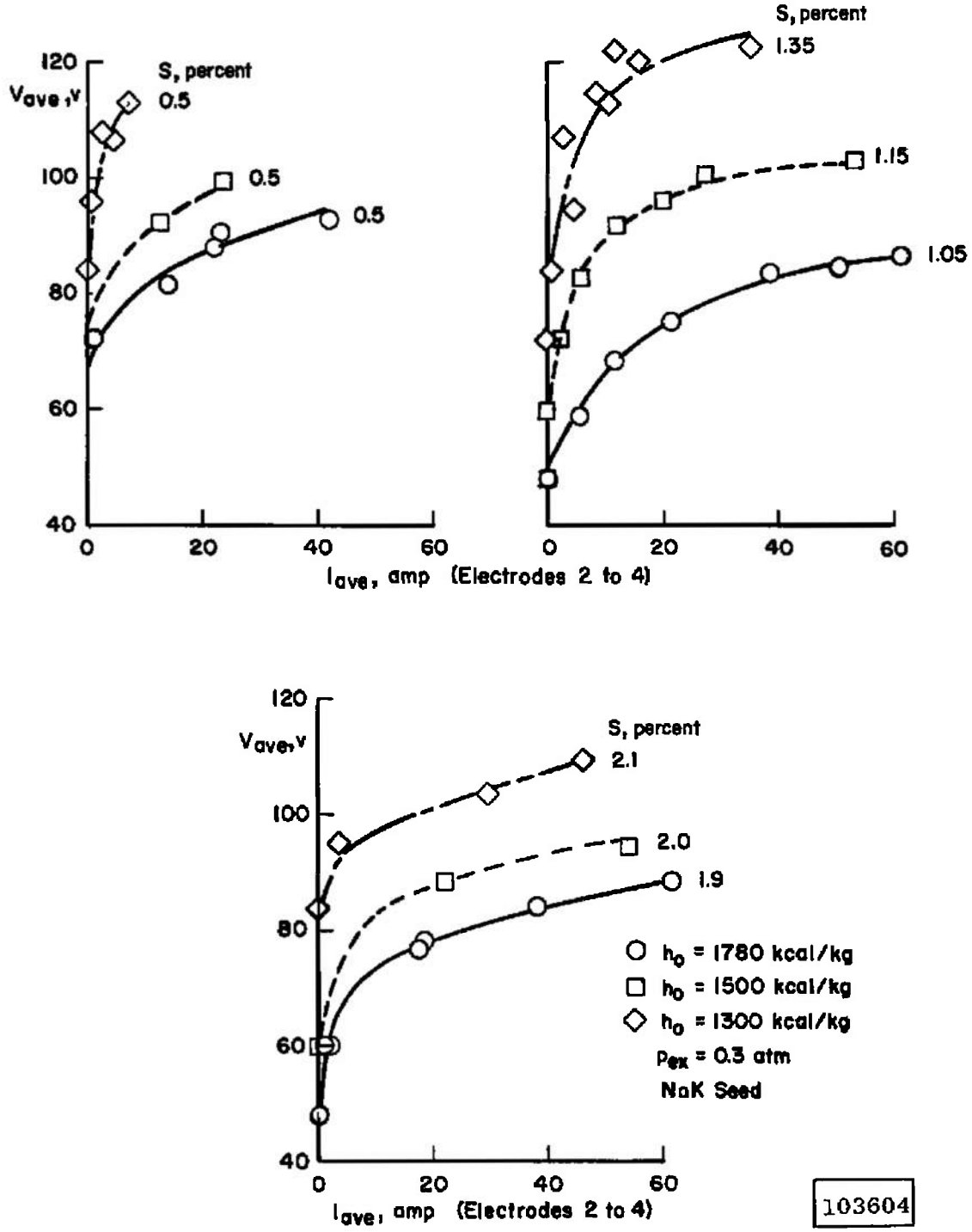

Fig. 19 Average Current-Voltage Characteristics of Channel 4 at Various Seed Rates and Enthalpy Levels

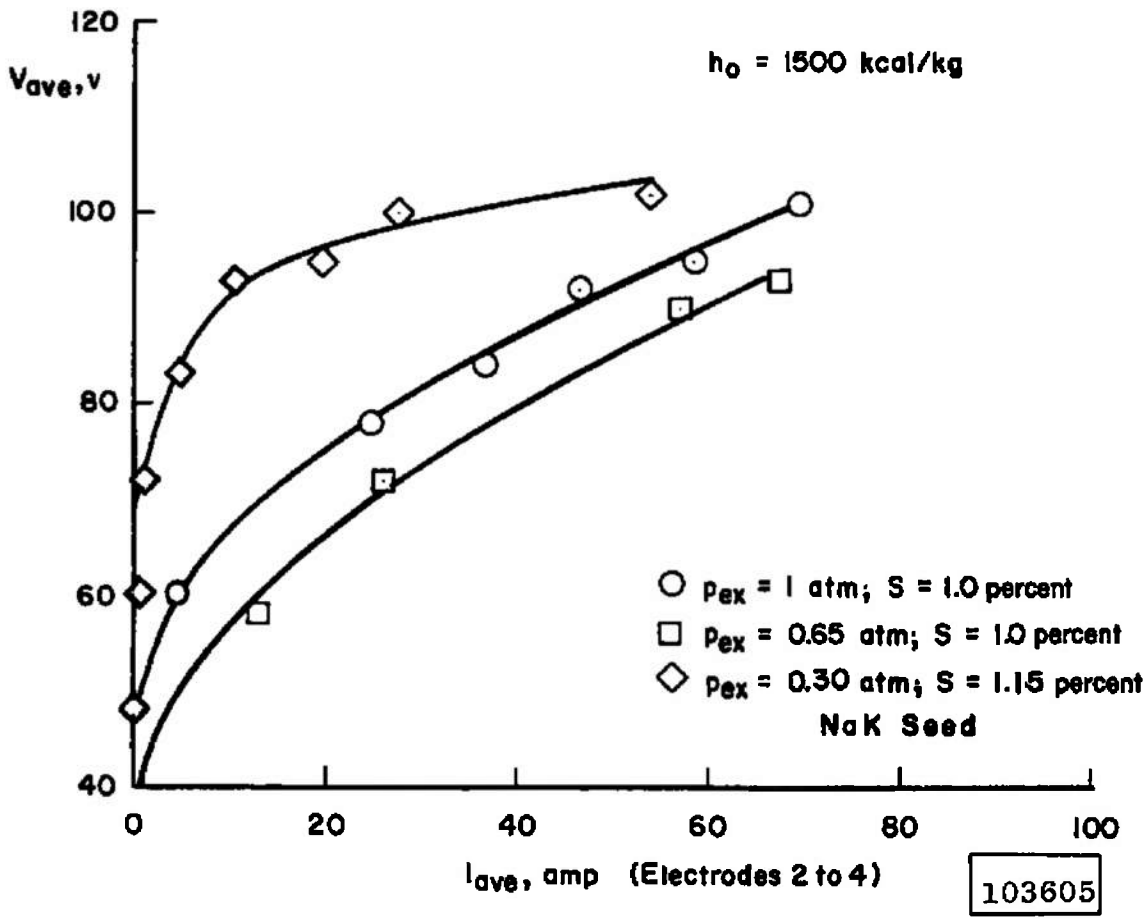

Fig. 20 Averaged Current-Voltage Characteristics of Channel 4 at Various Pressure Levels

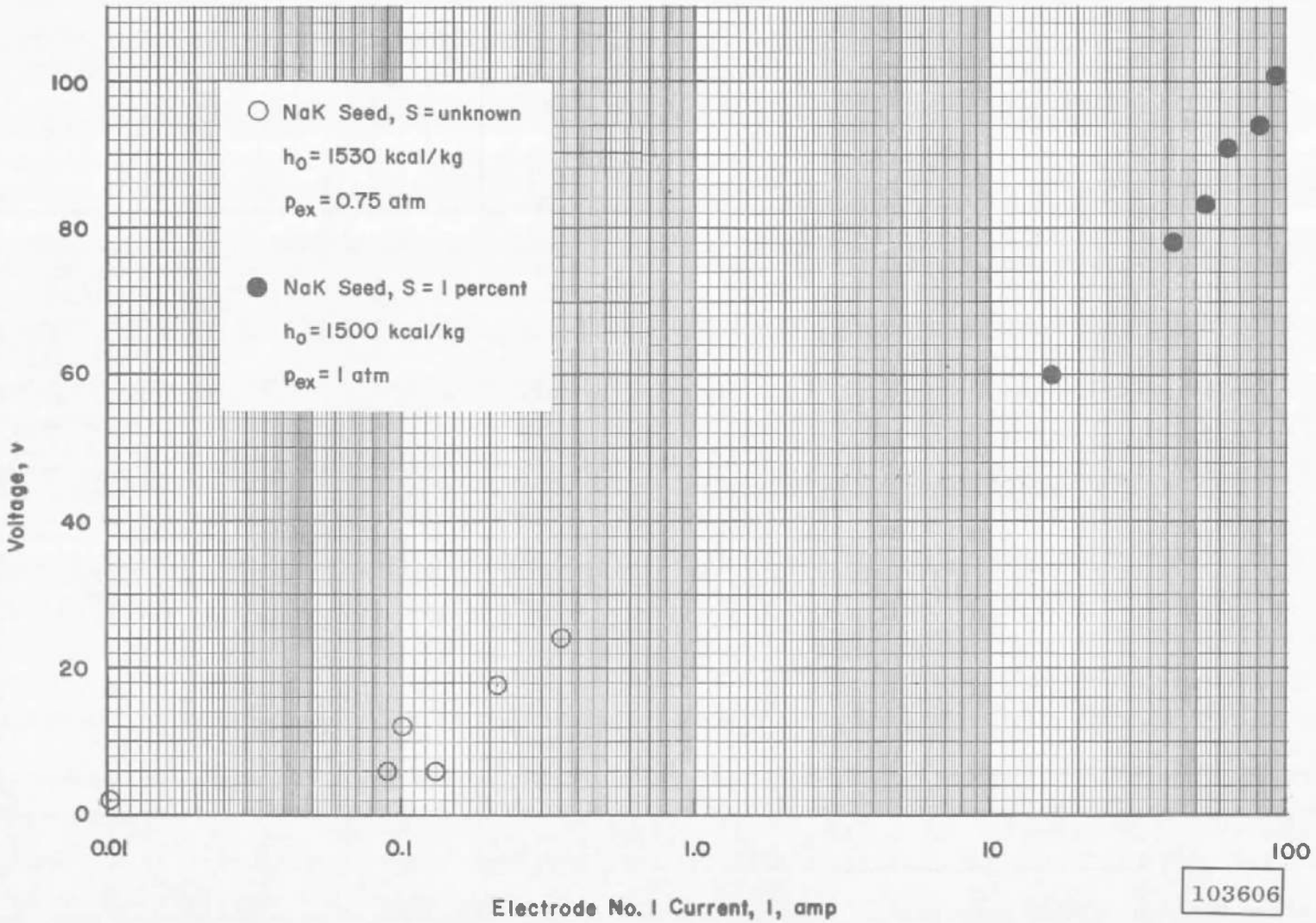

Fig. 21 Current-Voltage Characteristics of Channel 4 over a Large Current Range

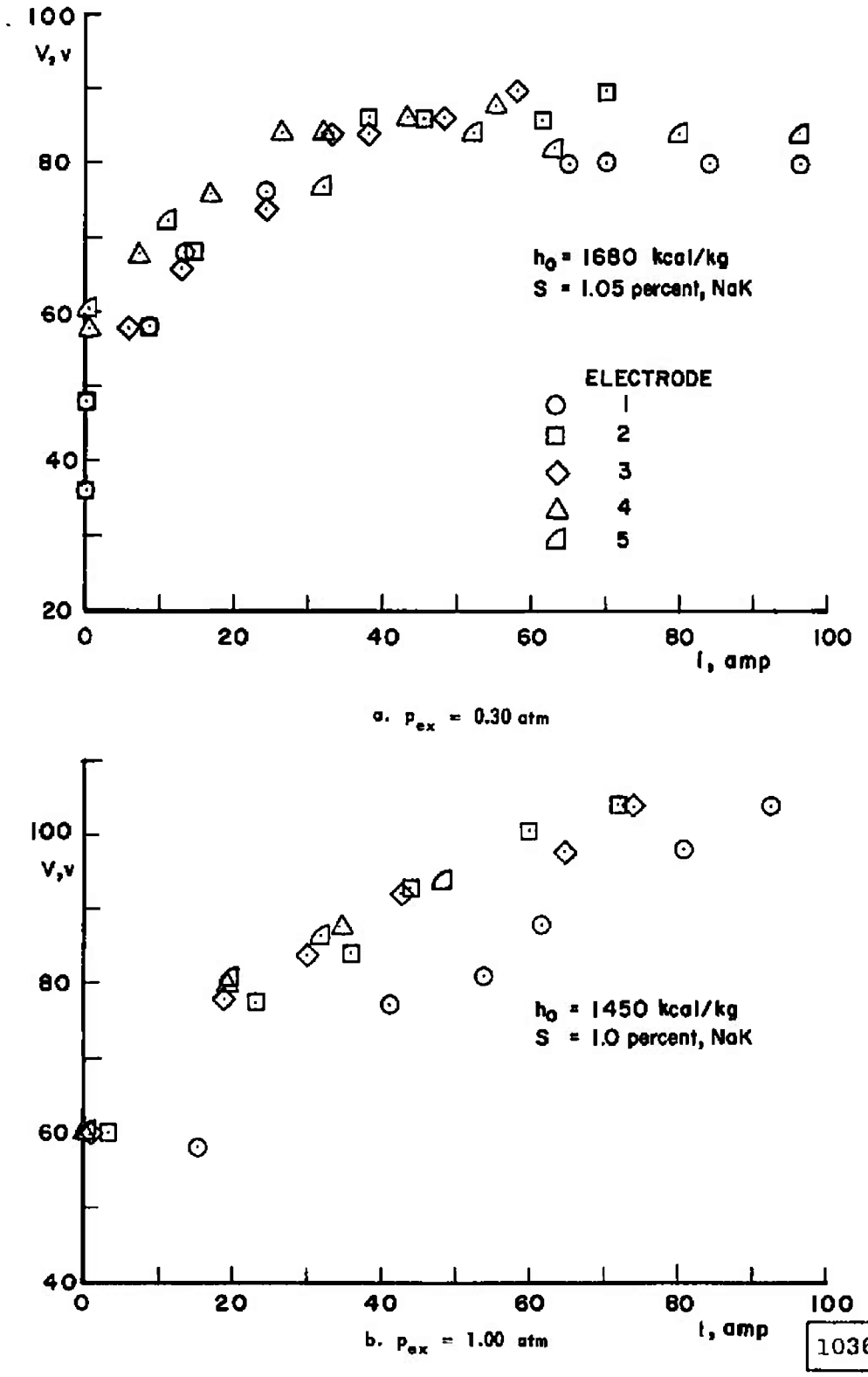

Fig. 22 Current-Voltage Characteristics for Various Electrode Pairs in Channel 4

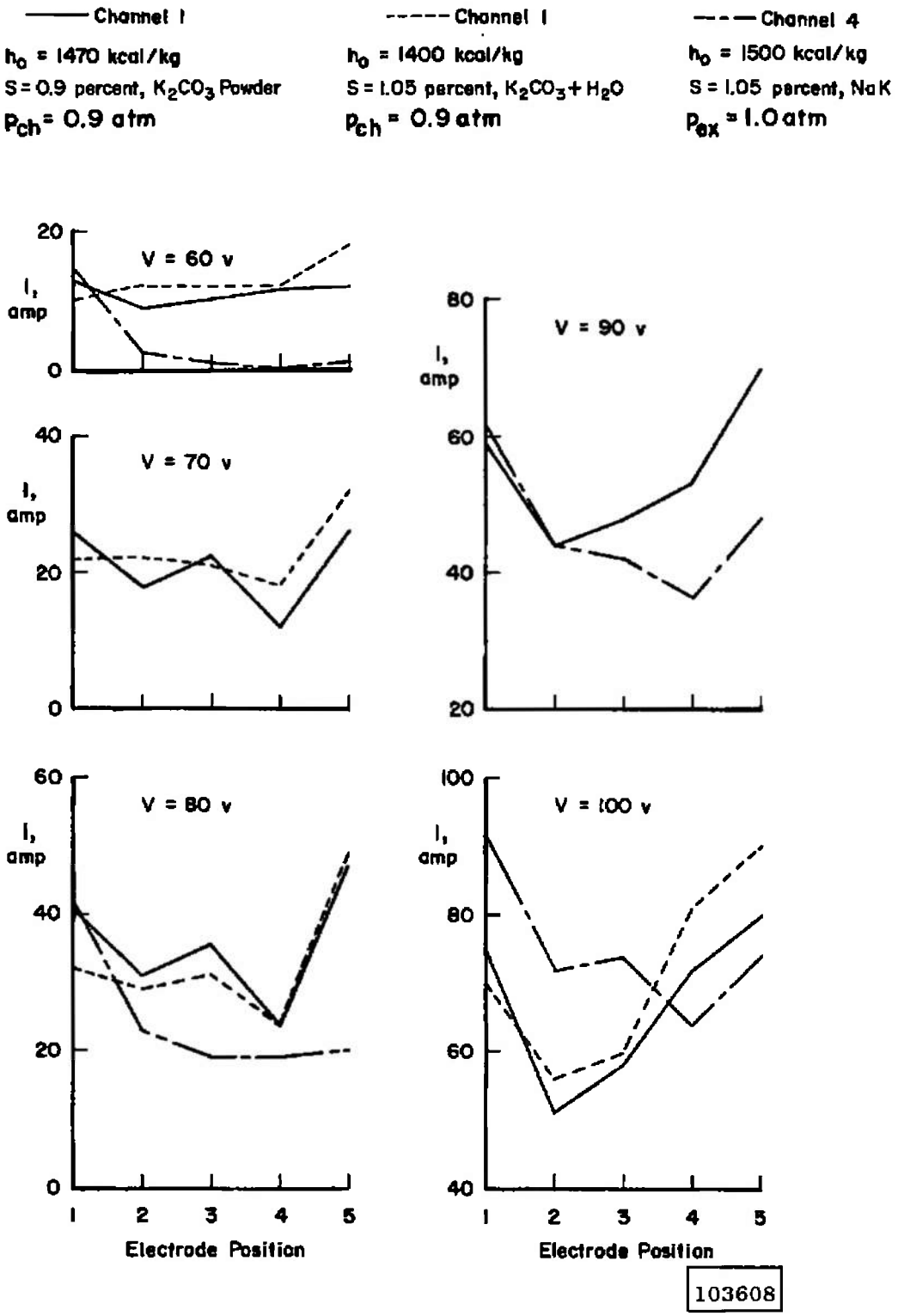

Fig. 23 Effect of Seed Type on the Current Distribution in the Axial Direction

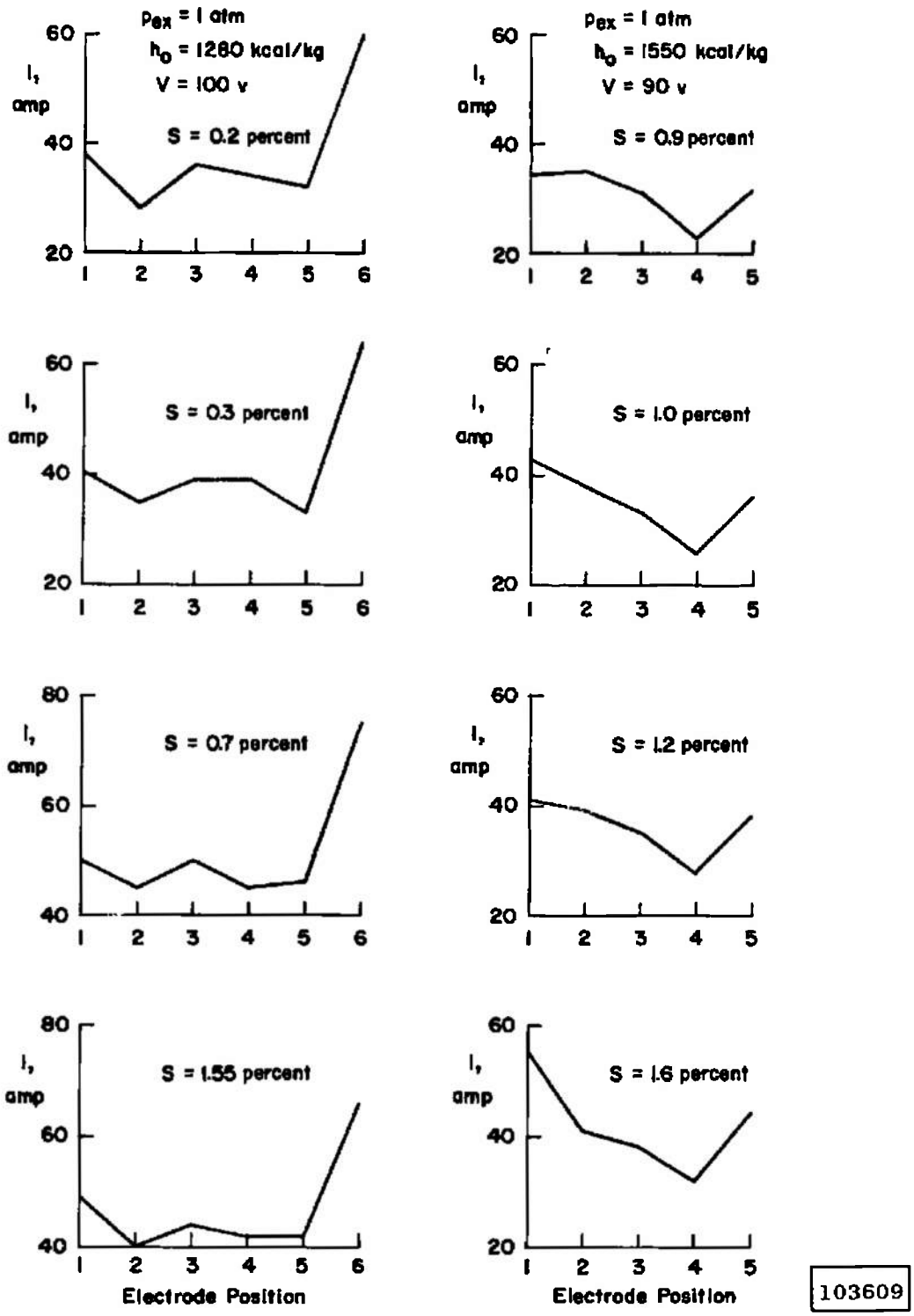

a. K_2CO_3 + H_2O Seed, Channel 3

b. NaK Seed, Channel 4

Fig. 24 Effect of Seeding Rate on the Current Distribution in the Axial Direction

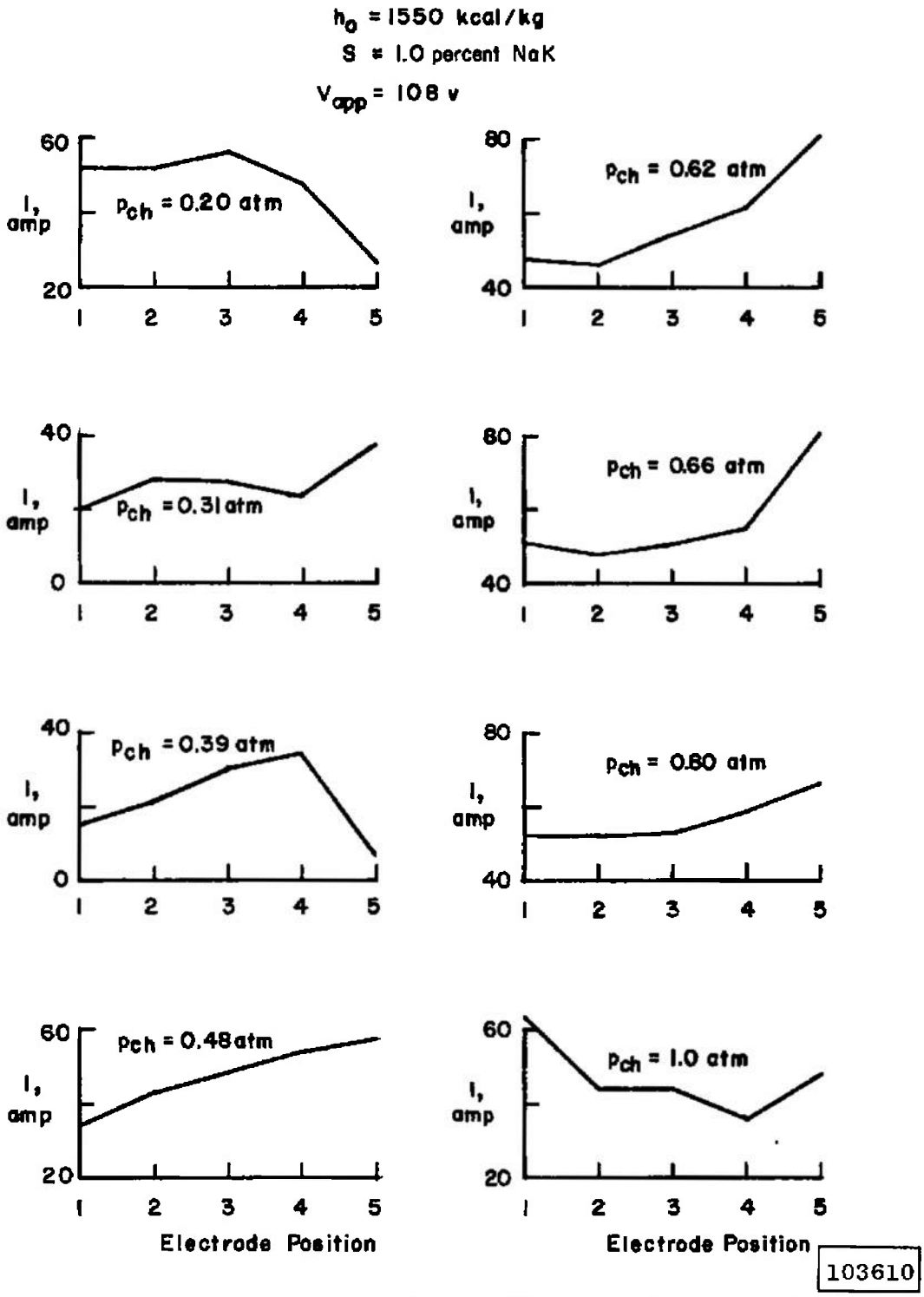

Fig. 25 Effect of Pressure Level on the Current Distribution in the Axial Direction

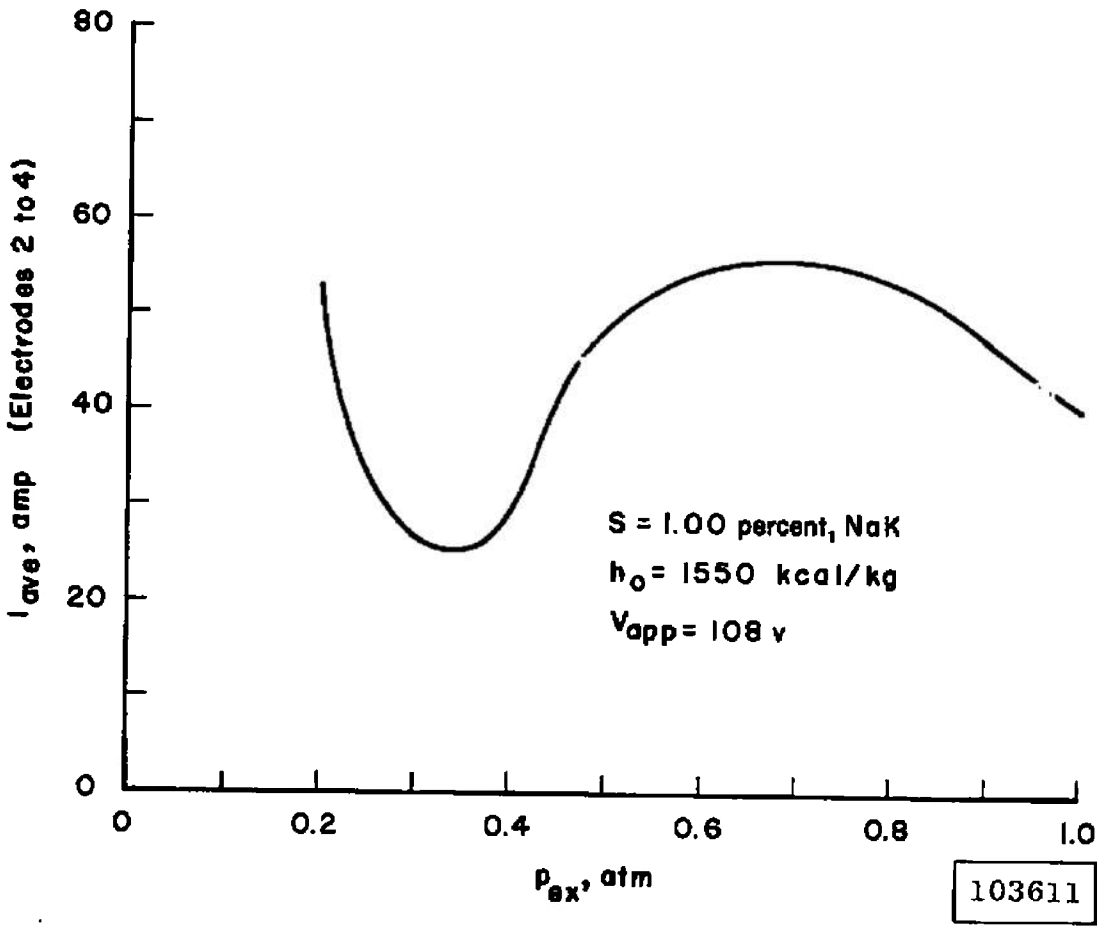

Fig. 26 Average Electrode Current as a Function of Pressure Level

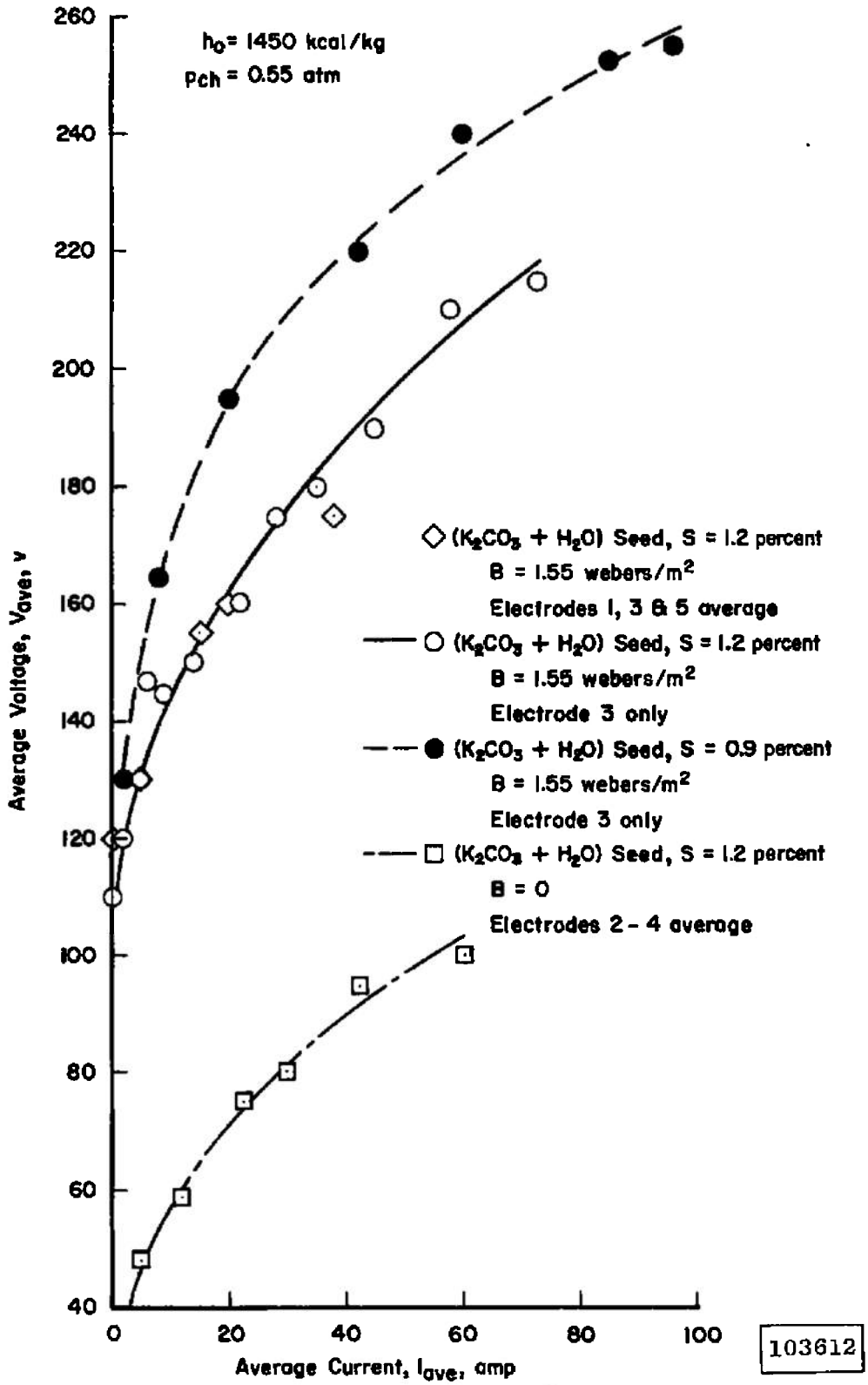

Fig. 27 Averaged Current-Voltage Characteristics of Channel 2 with and without an Applied Magnetic Field

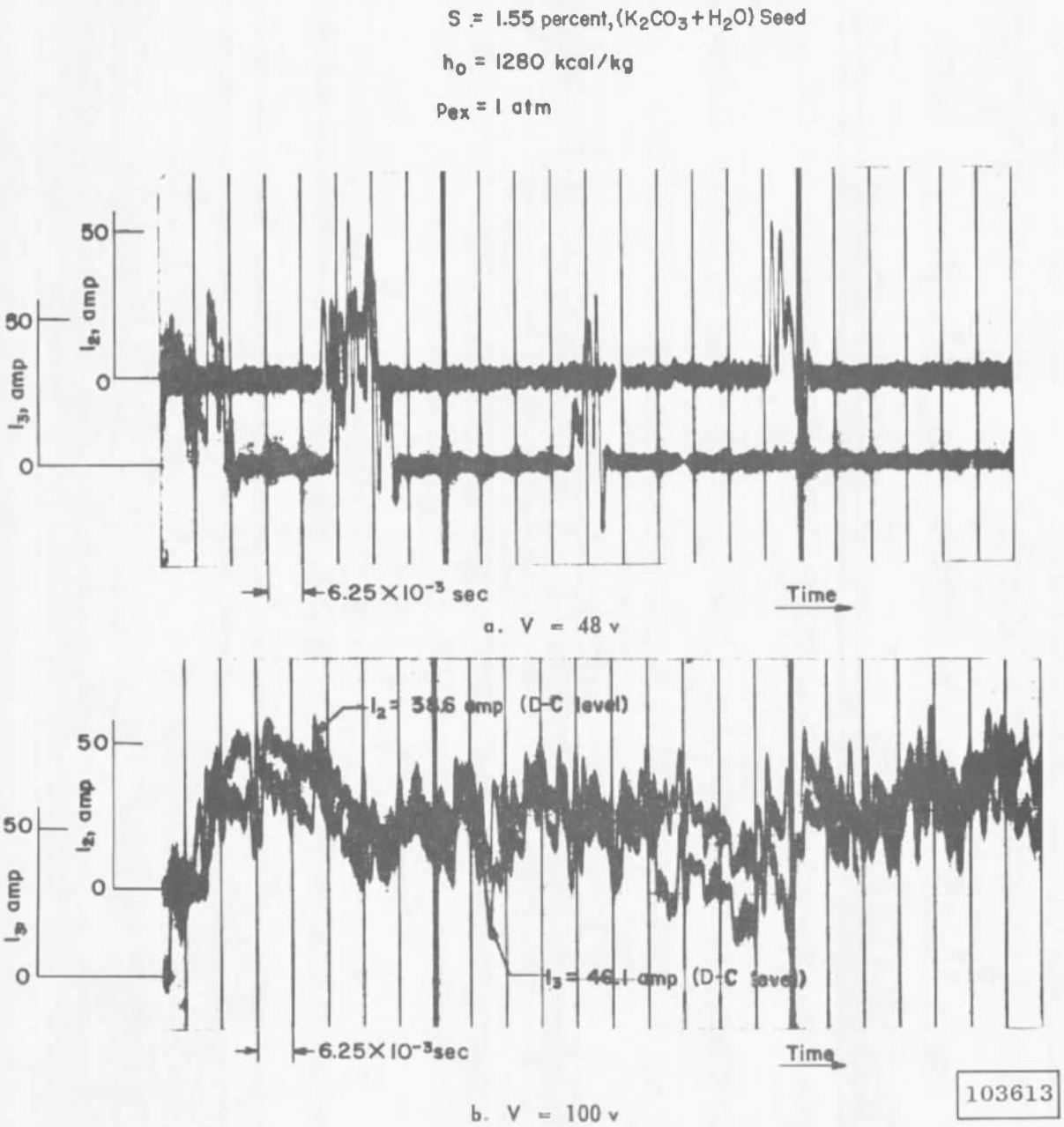

Fig. 28 High Frequency Current Fluctuations for Electrode Pairs 2 and 3 in Channel 3

B = 15,500 gauss

h_0 = 1550 kcal/kg

S = 1.24 percent, $K_2CO_3 + H_2O$

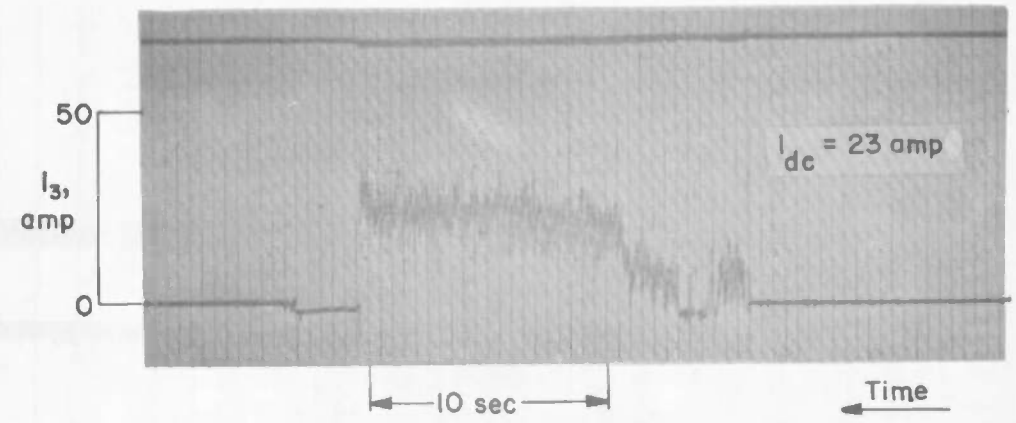

a. V = 164 v

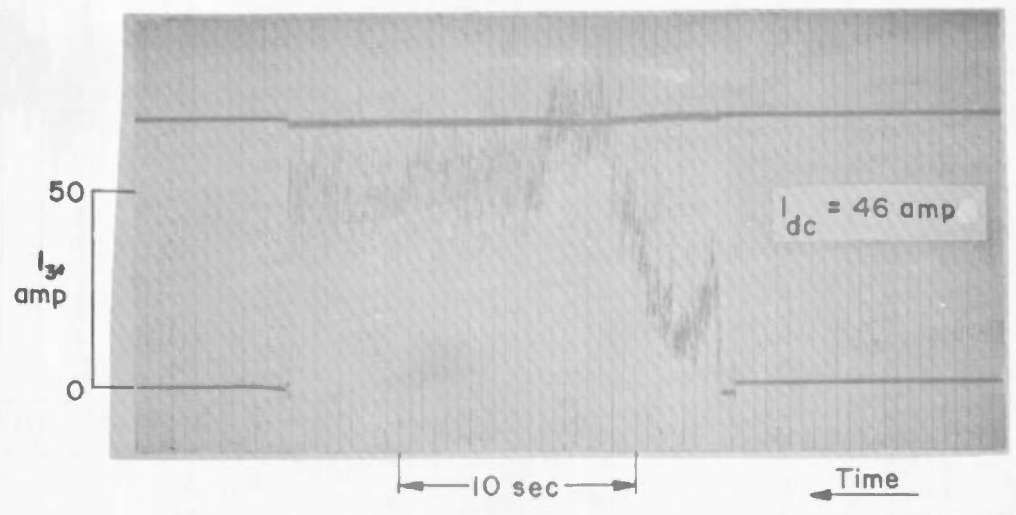

b. V = 195 v

Fig. 29 Current Fluctuations of Electrode Pair 3 in Channel 2 with a 15,500-gauss Magnetic Field

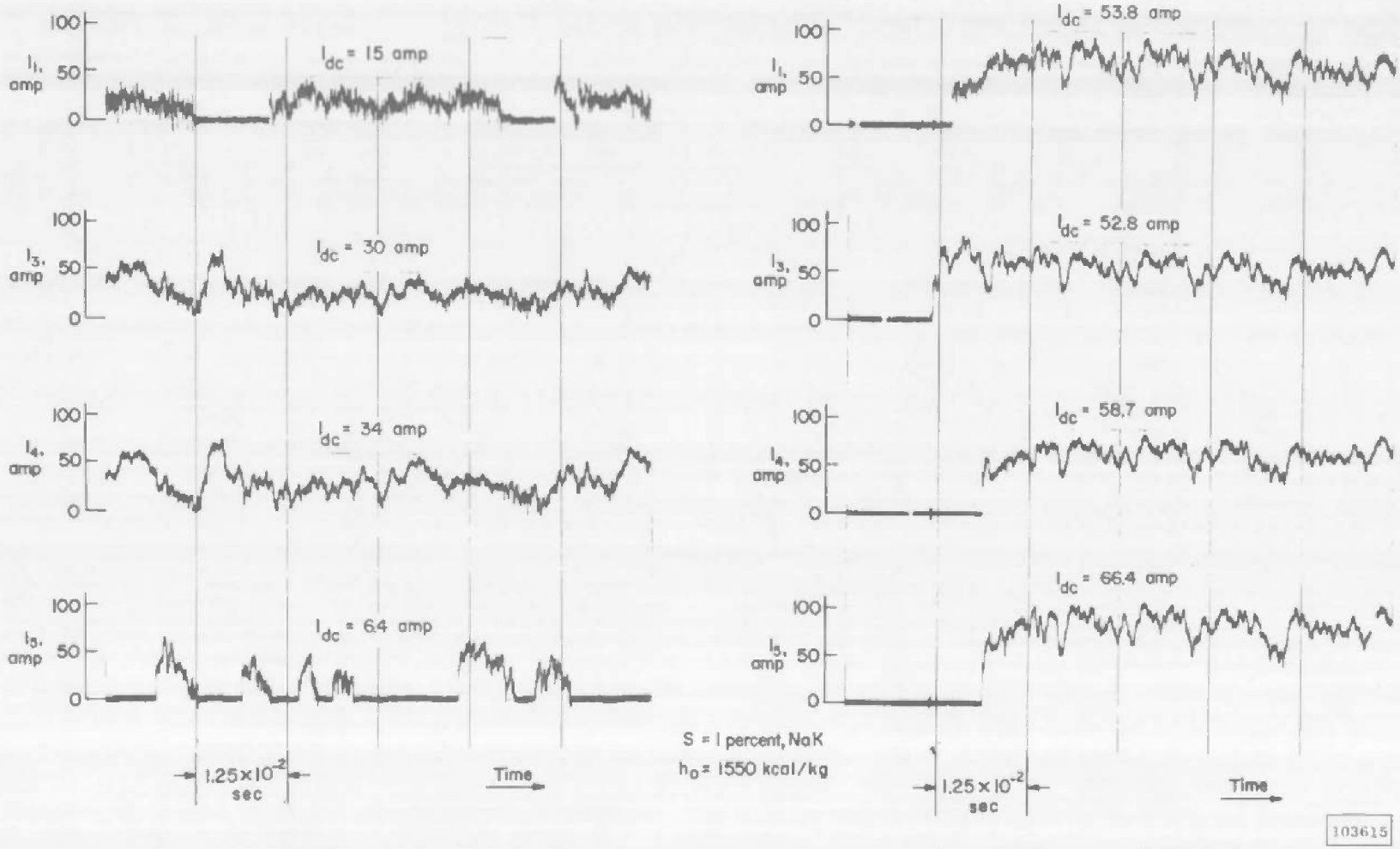

a. V = 100 v, p_{ch} = 0.39 atm

b. V = 90 v, p_{ch} = 0.88 atm

Fig. 30 High-Frequency Current Fluctuations in Channel 4 at Various Operating Conditions

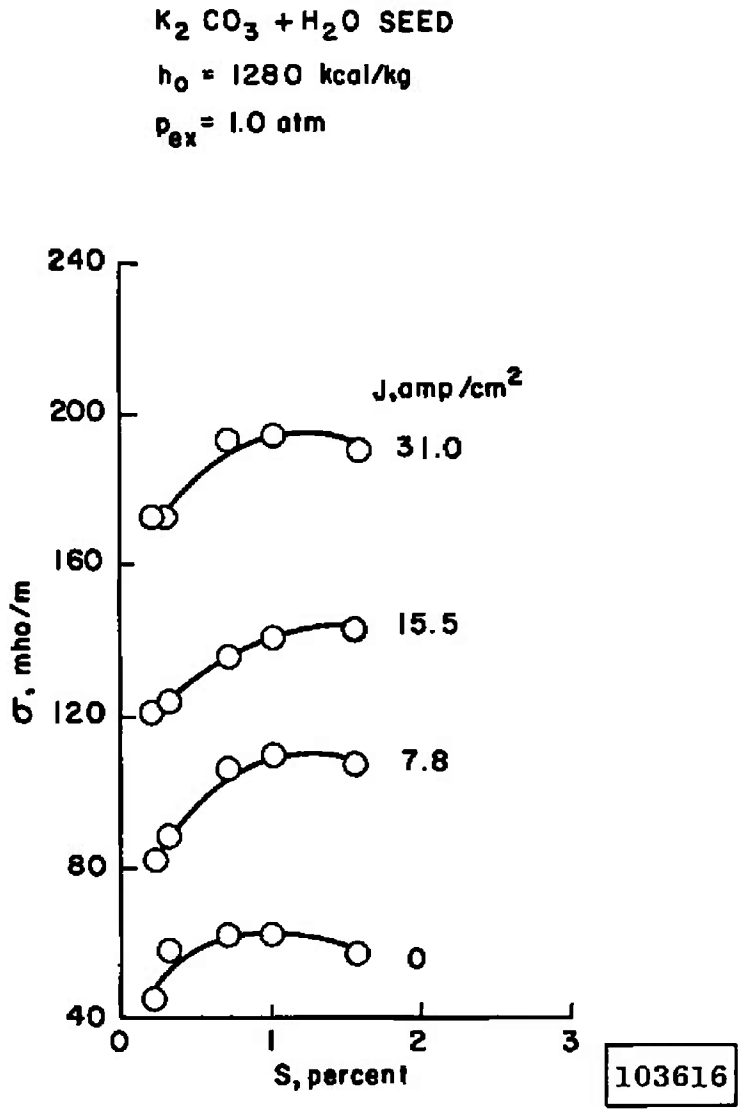

Fig. 31 Electrical Conductivity as a Function of Seed Rate at Various Current Densities

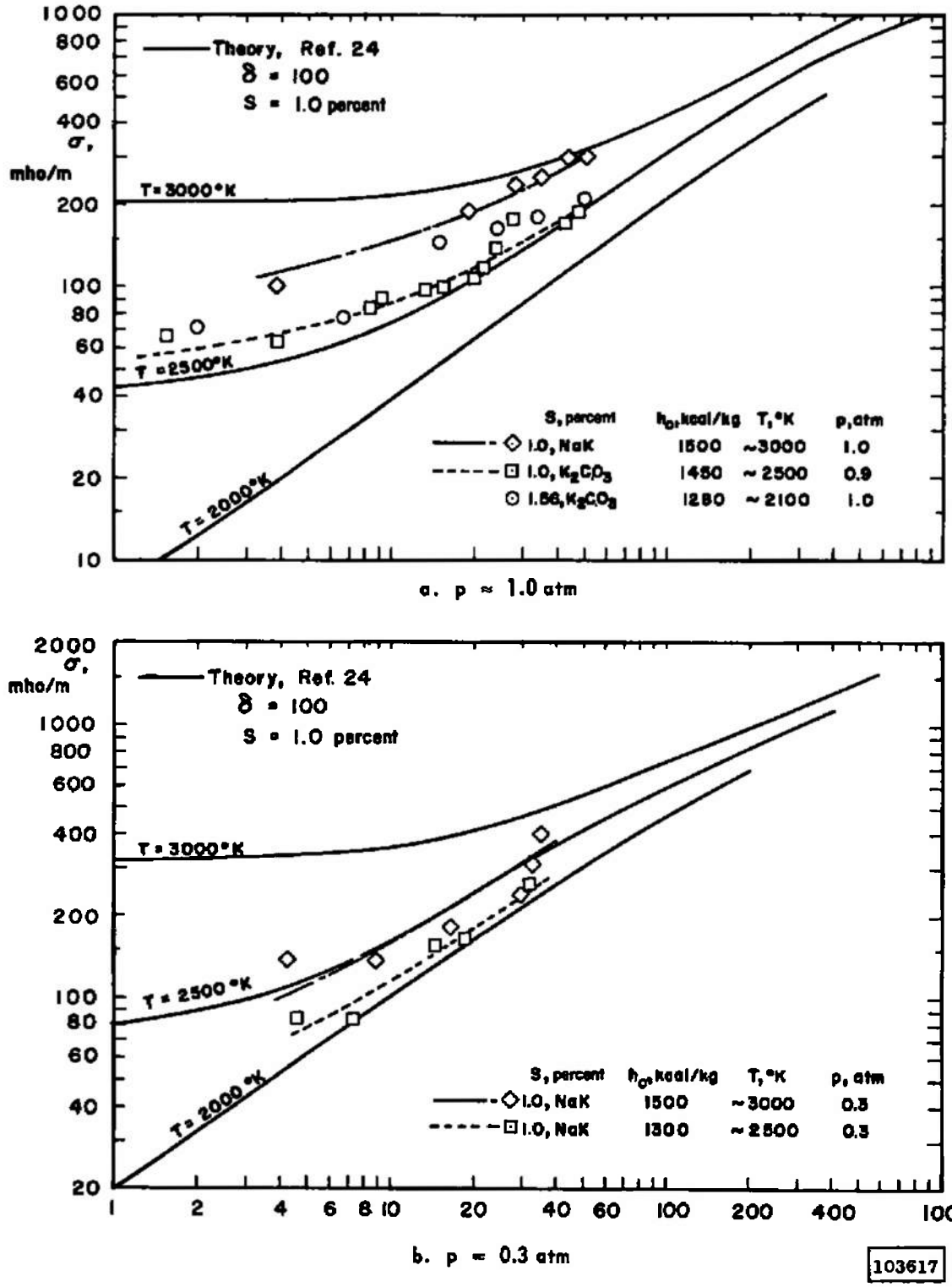

Fig. 32 Comparison of Electrical Conductivity with Nonequilibrium Electron Temperature Theory

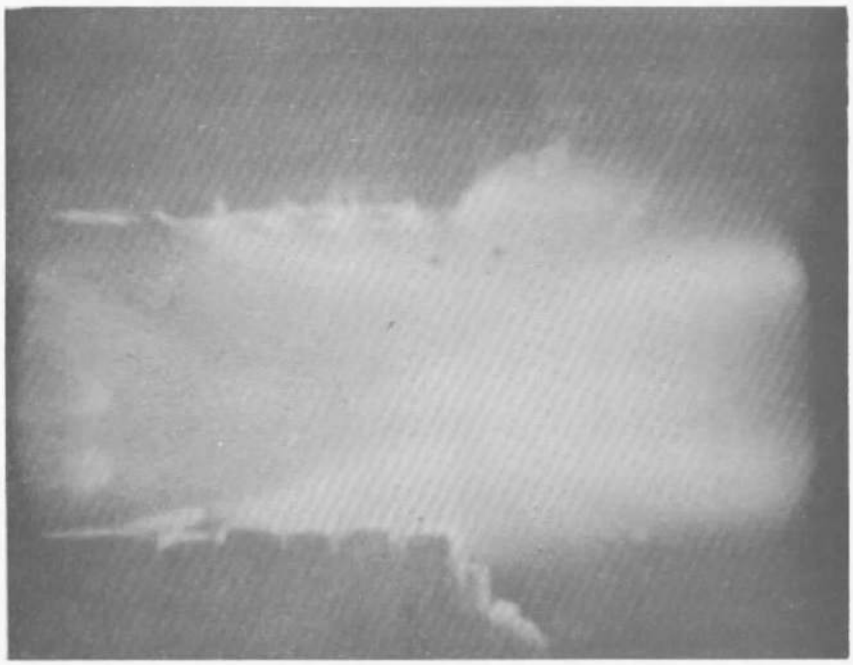

p_{ch} = 0.20 atm
h_o = 1550 kcal/kg
S = 1.0 % NaK
V_{ave} = 90 v
I_{ave} = 50 amp
B = 0

103618

Fig. 33 Electrical Discharge across Supersonic Seeded Plasma

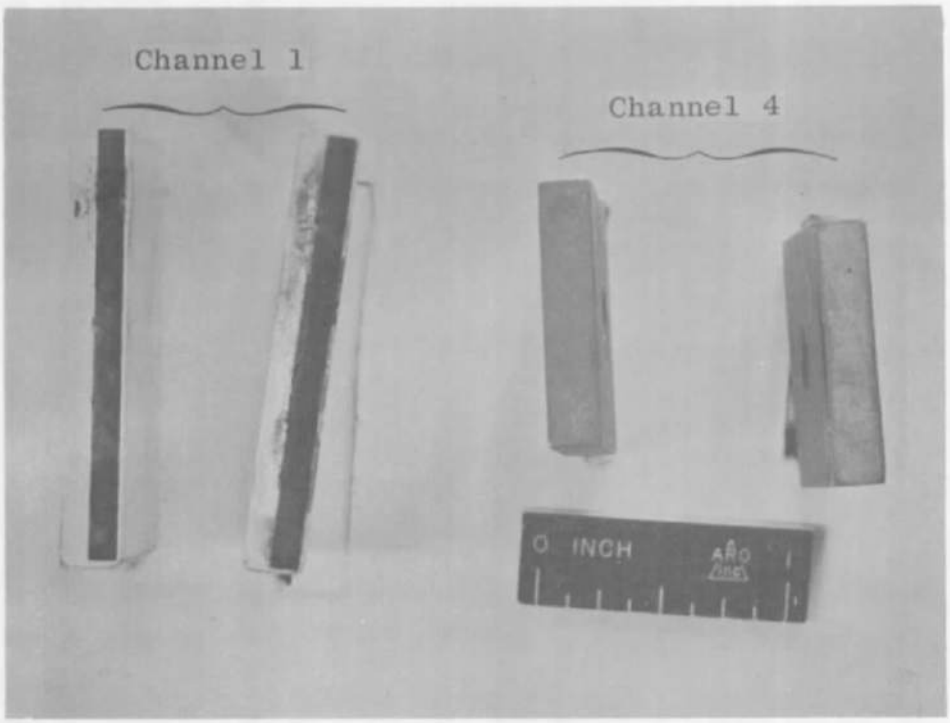

a. Copper Electrodes from Channels 1 and 4

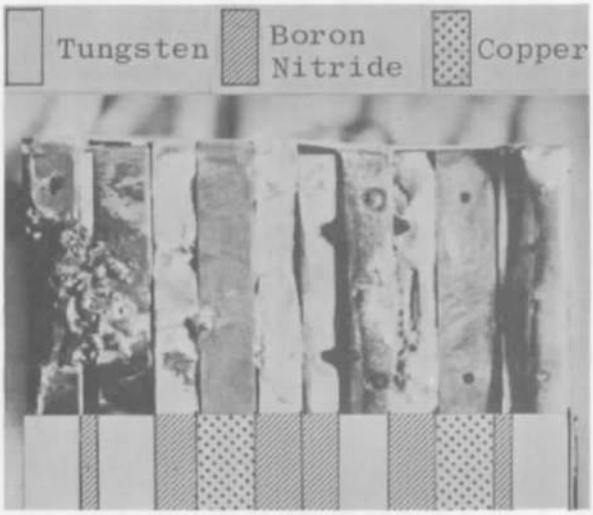

103619

b. Comparison of Electrode Erosion

Fig. 34 Characteristic Electrode Erosion

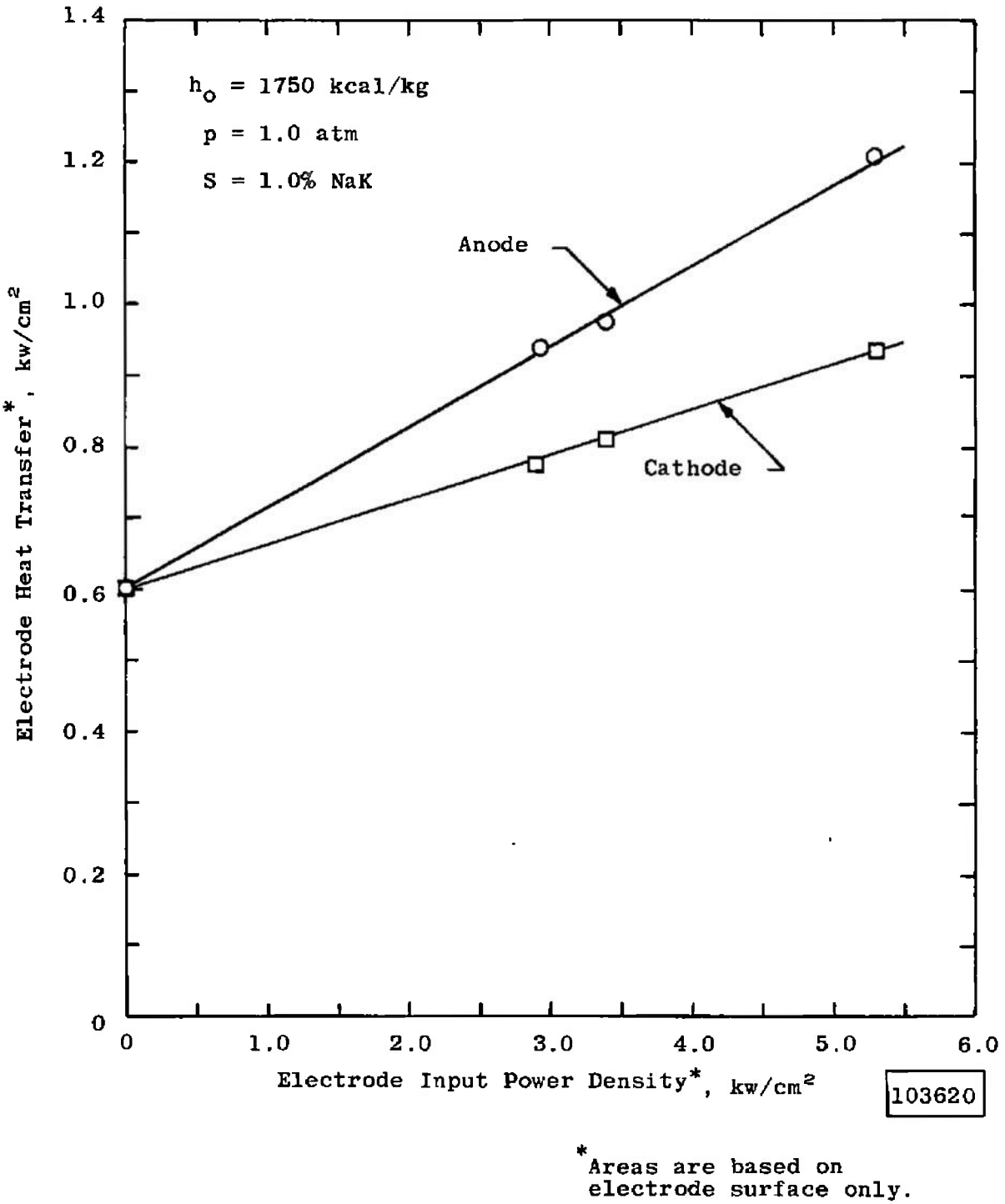

*Areas are based on electrode surface only.

Fig. 35 Electrode Heat-Transfer Rates

UNCLASSIFIED

Security Classification

DOCUMENT CONTROL DATA - R&D

(Security classification of title, body of abstract and indexing annotation must be entered when the overall report is classified)

1 ORIGINATING ACTIVITY (Corporate author)	2a REPORT SECURITY CLASSIFICATION
Arnold Engineering Development Center ARO, Inc., Operating Contractor Arnold Air Force Station, Tennessee	UNCLASSIFIED
	2b GROUP N/A

3 REPORT TITLE SOME CHARACTERISTICS OF AN ELECTRICAL DISCHARGE TRANSVERSE TO A SUPERSONIC SEEDED NITROGEN PLASMA STREAM WITH COLD-COPPER ELECTRODES

4 DESCRIPTIVE NOTES (Type of report and inclusive dates)
N/A

5 AUTHOR(S) (Last name, first name, initial)

K. E. Tempelmeyer, J. M. Whoric, L. E. Rittenhouse and M. L. McKee, ARO, Inc.

6 REPORT DATE	7a TOTAL NO OF PAGES	7b. NO OF REFS
March 1965	71	32

8a CONTRACT OR GRANT NO.	9a ORIGINATOR'S REPORT NUMBER(S)
AF 40(600)-1000 b. PROJECT NO. 7778 c. Program Element 62410034 d Task 777805	AEDC-TR-65-52
	9b. OTHER REPORT NO(S) (Any other numbers that may be assigned this report) N/A

10. AVAILABILITY/LIMITATION NOTICES
Qualified requesters may obtain copies of this report from DDC.

11 SUPPLEMENTARY NOTES	12. SPONSORING MILITARY ACTIVITY
N/A	Arnold Engineering Development Center, Air Force Systems Command, Arnold Air Force Station, Tennessee

13 ABSTRACT

Some characteristics of a steady, direct-current electrical discharge transverse to a supersonic seeded nitrogen plasma are presented. The discharge from cold-copper electrodes had an overall voltage-current characteristic which was positive in all cases. The effects of (1) the type of seed (K_2CO_3 or NaK), (2) the seeding rate (about 0.2 to 2 percent K or NaK by weight), (3) the static pressure level (from 0.3 to 1.0 atm), and (4) the plasma enthalpy level (from about 1250 to 1800 kcal/kg) on the discharge are given in figure form. Dynamic data were also recorded and demonstrate that rather large fluctuations having frequencies of a few hundred cps exist in the current. It is proposed that the electrodes introduce electrons into the conducting plasma through field emission. The discharge appears diffuse in the core of the plasma and may be quantitatively explained with an existing nonequilibrium, elevated-electron temperature theory.

DD FORM 1 JAN 64 1473

UNCLASSIFIED

Security Classification

14 KEY WORDS	LINK A		LINK B		LINK C	
	ROLE	WT	ROLE	WT	ROLE	WT
plasmas electric discharges cold-copper electrodes magnetohydrodynamic devices						

INSTRUCTIONS

1. ORIGINATING ACTIVITY: Enter the name and address of the contractor, subcontractor, grantee, Department of Defense activity or other organization *(corporate author)* issuing the report.

2a. REPORT SECURITY CLASSIFICATION: Enter the overall security classification of the report. Indicate whether "Restricted Data" is included. Marking is to be in accordance with appropriate security regulations.

2b. GROUP: Automatic downgrading is specified in DoD Directive 5200.10 and Armed Forces Industrial Manual. Enter the group number. Also, when applicable, show that optional markings have been used for Group 3 and Group 4 as authorized.

3. REPORT TITLE: Enter the complete report title in all capital letters. Titles in all cases should be unclassified. If a meaningful title cannot be selected without classification, show title classification in all capitals in parenthesis immediately following the title.

4. DESCRIPTIVE NOTES: If appropriate, enter the type of report, e.g., interim, progress, summary, annual, or final. Give the inclusive dates when a specific reporting period is covered.

5. AUTHOR(S): Enter the name(s) of author(s) as shown on or in the report. Enter last name, first name, middle initial. If military, show rank and branch of service. The name of the principal author is an absolute minimum requirement.

6. REPORT DATE: Enter the date of the report as day, month, year, or month, year. If more than one date appears on the report, use date of publication.

7a. TOTAL NUMBER OF PAGES: The total page count should follow normal pagination procedures, i.e., enter the number of pages containing information.

7b. NUMBER OF REFERENCES: Enter the total number of references cited in the report.

8a. CONTRACT OR GRANT NUMBER: If appropriate, enter the applicable number of the contract or grant under which the report was written.

8b, 8c, & 8d. PROJECT NUMBER: Enter the appropriate military department identification, such as project number, subproject number, system numbers, task number, etc.

9a. ORIGINATOR'S REPORT NUMBER(S): Enter the official report number by which the document will be identified and controlled by the originating activity. This number must be unique to this report.

9b. OTHER REPORT NUMBER(S): If the report has been assigned any other report numbers *(either by the originator or by the sponsor)*, also enter this number(s).

10. AVAILABILITY/LIMITATION NOTICES: Enter any limitations on further dissemination of the report, other than those imposed by security classification, using standard statements such as:

(1) "Qualified requesters may obtain copies of this report from DDC."

(2) "Foreign announcement and dissemination of this report by DDC is not authorized."

(3) "U. S. Government agencies may obtain copies of this report directly from DDC. Other qualified DDC users shall request through _____."

(4) "U. S. military agencies may obtain copies of this report directly from DDC. Other qualified users shall request through _____."

(5) "All distribution of this report is controlled. Qualified DDC users shall request through _____."

If the report has been furnished to the Office of Technical Services, Department of Commerce, for sale to the public, indicate this fact and enter the price, if known.

11. SUPPLEMENTARY NOTES: Use for additional explanatory notes.

12. SPONSORING MILITARY ACTIVITY: Enter the name of the departmental project office or laboratory sponsoring *(paying for)* the research and development. Include address.

13. ABSTRACT: Enter an abstract giving a brief and factual summary of the document indicative of the report, even though it may also appear elsewhere in the body of the technical report. If additional space is required, a continuation sheet shall be attached.

It is highly desirable that the abstract of classified reports be unclassified. Each paragraph of the abstract shall end with an indication of the military security classification of the information in the paragraph, represented as *(TS)*, *(S)*, *(C)*, or *(U)*.

There is no limitation on the length of the abstract. However, the suggested length is from 150 to 225 words.

14. KEY WORDS: Key words are technically meaningful terms or short phrases that characterize a report and may be used as index entries for cataloging the report. Key words must be selected so that no security classification is required. Identifiers, such as equipment model designation, trade name, military project code name, geographic location, may be used as key words but will be followed by an indication of technical context. The assignment of links, rules, and weights is optional.